Nature of the Chromophore Binding Site of Bacteriorhodopsin: The Potential Role of Arg^{82} as a Principal Counterion

Anakarin Kusnetzow, Deepak L. Singh, Charles H. Martin, Igor J. Barani, and Robert R. Birge
Department of Chemistry and W. M. Keck Center for Molecular Electronics, Syracuse University, Syracuse, New York 13244 USA

ABSTRACT The nature of the chromophore binding site of light-adapted bacteriorhodopsin is analyzed by using modified neglect of differential overlap with partial single and double configuration interaction (MNDO-PSDCI) molecular orbital theory to interpret previously reported linear and nonlinear optical spectroscopic measurements. We conclude that in the absence of divalent metal cations in close interaction with Asp^{85} and Asp^{212}, a positively charged amino acid must be present in the same vicinity. We find that models in which Arg^{82} is pointed upward into the chromophore binding site and directly stabilizes Asp^{85} and Asp^{212} are successful in rationalizing the observed one-photon and two-photon properties. We conclude further that a water molecule is strongly hydrogen bonded to the chromophore imine proton. The chromophore "$^1B_u^{*+}$" and "$^1A_g^{*-}$" states, despite extensive mixing, exhibit significantly different configurational character. The lowest-lying "$^1B_u^{*+}$" state is dominated by single excitations, whereas the second-excited "$^1A_g^{*-}$" state is dominated by double excitations. We can rule out the possibility of a negatively charged binding site, because such a site would produce a lowest-lying "$^1A_g^{*-}$" state, which is contrary to experimental observation. The possibility that Arg^{82} migrates toward the extracellular surface during the photocycle is examined.

INTRODUCTION

Bacteriorhodopsin is the light-transducing protein in the purple membrane of *Halobacterium salinarium* (also called *Halobacterium halobium*) (Oesterhelt and Schuhmann, 1974; Oesterhelt and Stoeckenius, 1971, 1974; Stoeckenius and Bogomolni, 1982). Upon the absorption of light, bacteriorhodopsin converts from a dark-adapted state (bR^{DA}), containing a mixture of 13-*cis* and all-*trans* chromophores, to a light-adapted state (bR^{LA}) that contains only the all-*trans* chromophore (Fig. 1). Subsequent absorption of light by the light-adapted state initiates a photocycle that pumps protons across the membrane, with a net transport from the inside (cytoplasmic) to the outside (extracellular) surfaces. The resulting pH gradient ($\Delta pH \approx 1$) generates a protonmotive force that is used by the bacterium to synthesize ATP from inorganic phosphate and ADP.

The nature of the bacteriorhodopsin binding site remains a subject of intense study and limited consensus. Of particular interest here is the counterion environment, which determines the net charge on the binding site and plays a significant role in directing the photochemical isomeric composition (Chronister and El-Sayed, 1987; Fischer et al., 1981; Koyama et al., 1993; Maeda et al., 1981; Mowery et al., 1979; Tallent et al., 1998). Two-photon spectroscopy is a particularly sensitive spectroscopic technique for probing the electrostatic nature of chromophore binding sites, because it allows assignment of the location and properties of low-lying forbidden states that respond to local electrostatic fields in a way that is very different from that of the one-photon allowed excited states (Birge, 1986; Birge et al., 1985; Birge and Zhang, 1990; Stuart et al., 1995). Two-photon spectroscopy was the first technique to demonstrate that the binding site of rhodopsin was neutral (Birge et al., 1985), and this conclusion was subsequently verified by site-directed mutagenesis studies (Sakmar et al., 1989; Zhukovsky and Oprian, 1989). When we initiated our studies of bacteriorhodopsin more than a decade ago, we anticipated that this nonlinear technique would provide new insights into the electrostatic characteristics of the binding site of bacteriorhodopsin. As discussed in our initial study, we were unable to assign a definitive model that could accommodate the spectroscopic data. Four observations were possible: 1) the chromophore is protonated, 2) the binding site is very ionic and may be charged, 3) there are no bare charges near the β-ionylidene ring, and 4) at least one water molecule interacts strongly with the imine proton of the chromophore (Birge and Zhang, 1990). Our best model predicted a neutral binding site with a water molecule hydrogen bonded to the protonated Schiff base imine proton and a single negative counterion, Asp^{212} (Birge and Zhang, 1990). The initial two-photon study was completed before the publication of the 3.5-Å diffraction study of bacteriorhodopsin by Henderson and co-workers (Grigorieff et al., 1996; Henderson et al., 1990a,b). The diffraction data provided evidence for two aspartic acid residues near the imine linkage (Asp^{85} and Asp^{212} and two tyrosine residues (Tyr^{57} and Tyr^{185}) inside the binding site). At that time, there was controversy regarding the protonation states of the tyrosine residues (Ames et al., 1990, 1992; Duñach et al., 1990a; Harada et al., 1990; Herzfeld et al., 1990; McDermott et al., 1991; Roepe et al., 1988; Rothschild et al., 1990). A subsequent reanalysis of the two-photon data using the "Henderson model" as a starting point concluded that Tyr^{57} and Tyr^{185} were both protonated, but if both Asp^{85} and Asp^{212}

Received for publication 4 September 1998 and in final form 13 February 1999.

Address reprint requests to Dr. Robert R. Birge, Department of Chemistry, Syracuse University, 111 College Place, Syracuse, NY 13244-4100. Tel.: 315-443-1900; Fax: 315-443-4070; E-mail: rbirge@syr.edu.

0006-3495/99/05/2370/20 $2.00

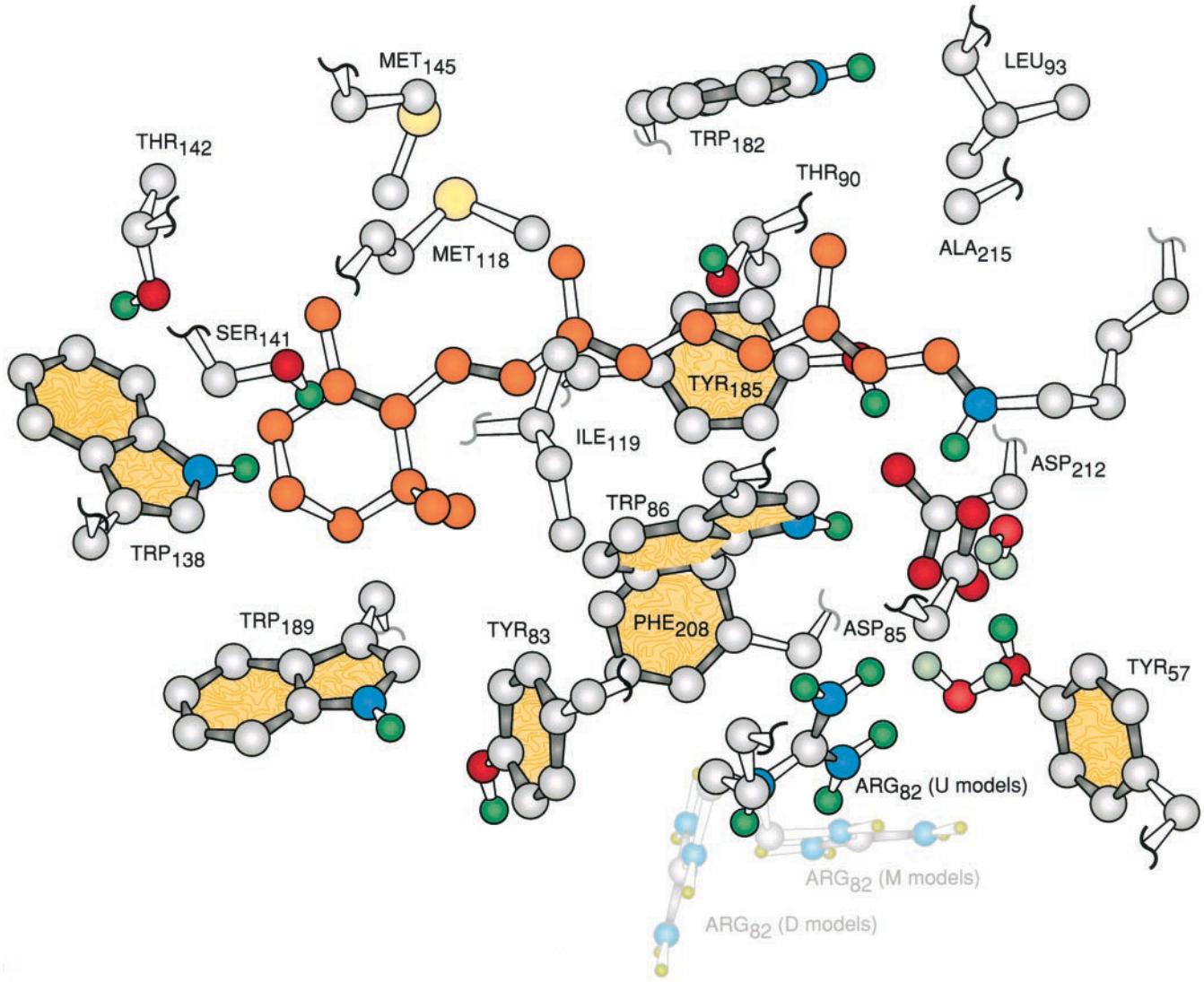

FIGURE 1 The chromophore and surrounding amino acids that make up the chromophore binding site of light-adapted bacteriorhodopsin. The coordinates are taken from the 2.3-Å structure kindly provided to us by Drs. Lanyi and Luecke, based on their study published in Luecke et al. (1998). The side chain of the Arg^{82} residue is shown in the various positions associated with the models listed in parentheses.

were unprotonated, a counterion had to be present within the binding site to mediate the charge (Stuart et al., 1995). We proposed that a Ca(II) ion is in electrostatic contact with the two aspartic acid residues (Asp^{85} and Asp^{212}) (Fig. 2) (Stuart et al., 1995). This model reproduces the one-photon and two-photon properties while simultaneously accommodating or helping to rationalize a host of other spectroscopic, chemical, and mutagenic studies (Ariki et al., 1987; Birge et al., 1996; El-Sayed et al., 1995; Jonas and Ebrey, 1991; Masuda et al., 1995; Sweetman and El-Sayed, 1991; Tan et al., 1996; Zhang and El-Sayed, 1993; Zhang et al., 1992, 1993). We concluded that this chromophore-adjacent cation binding site was the second high-affinity calcium binding site and represented the color-controlling site originally predicted by Jonas and Ebrey (1991).

We were prompted to reexamine the divalent cation-based binding site in light of a recent study by Fu et al. (1997), which examined the kinetics of Asp^{85} reprotonation as a function of cation properties. These studies suggest that the color-controlling cation binding site is in an exposed location on or close to the membrane surface. Although it does not directly rule out calcium in a chromophore-adjacent cation binding site, this study places rather severe constraints that question the feasibility of this model. Further inspiration for the present study is the observation that none of the more recent, high-resolution diffraction studies identify a divalent cation within the chromophore binding site (Kimura et al., 1997a,b; Luecke et al., 1998; Pebay-Peyroula et al., 1997). Although the inability to find a metal cation in the binding site could be rationalized by the rapid motion of a Ca(II) or Mg(II) ion between two conformational minima, the observation of discrete water molecules in the same region (Luecke et al., 1998; Pebay-Peyroula et al., 1997) would argue against such an explanation. In contrast, a more recent paper by Pardo et al. presents a model for the binding site based on superconducting quan-

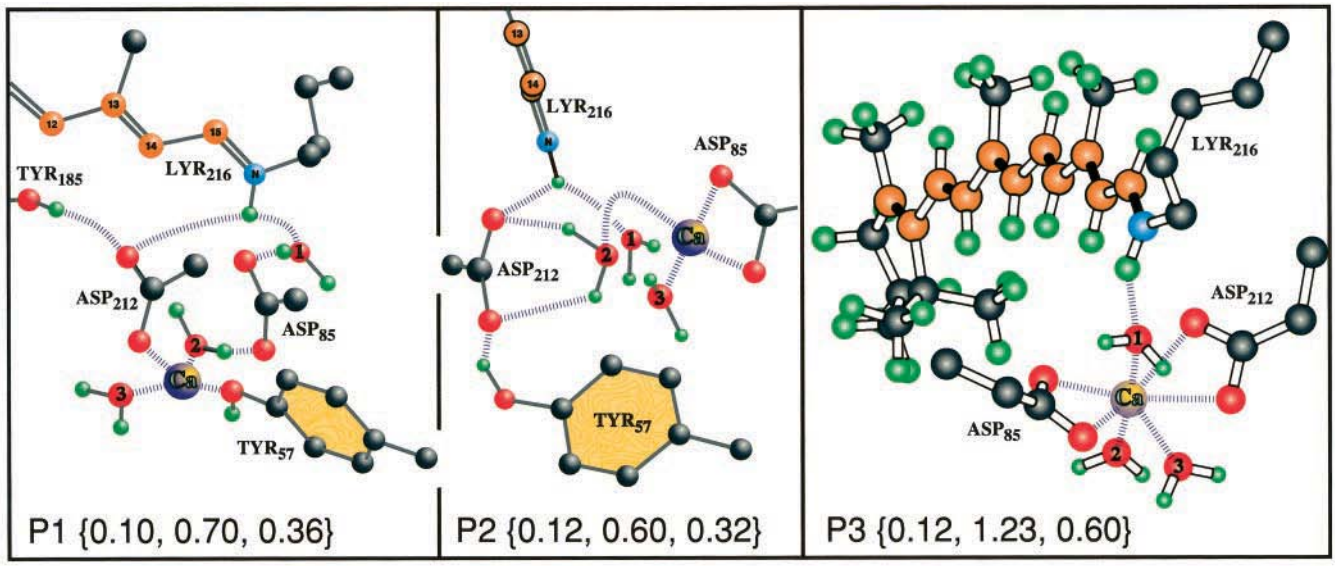

FIGURE 2 Three models of the chromophore binding site, which involve participation of a metal cation and produce a positively charged site. The two chromophore binding site models, P1 and P2, were proposed in our previous study (after Stuart et al., 1995). Model P3 was recently proposed based on superconducting quantum magnetometry and ab initio molecular orbital theory (Pardo et al., 1998). The numbers in curly braces give the one-photon error (Eq. 3), the two-photon error (Eq. 4), and the total error (Eq. 5), $\{\epsilon_{\text{one-photon}}, \epsilon_{\text{two-photon}}, \epsilon_{\text{total}}\}$, with all data taken from Table 2.

tum magnetometry in which a divalent metal, Mg(II) or Ca(II), is in direct interaction with both Asp^{85} and Asp^{212} (Pardo et al., 1998). Coupled with this inconsistency is the observation that the three recent diffraction studies predict a very different counterion environment for the chromophore and, in at least one case, require the presence of an additional (unspecified) cationic group to rationalize the observed electronic properties (see below).

We have long argued that the two-photon data are inconsistent with a negatively charged binding site (Birge and Zhang, 1990; Stuart et al., 1995). Thus a positively charged counterion must be in the electrostatic vicinity of the chromophore. If a metal cation is not present in the binding site, then the most realistic possibility is Arg^{82}, as first proposed by Braiman et al. (1988). A number of experimental and theoretical studies are consistent with this assumption (Alexiev et al., 1994; Balashov et al., 1993, 1995; Braiman et al., 1988; de Groot et al., 1990; Dér et al., 1991; Humphrey et al., 1994; Marti et al., 1991; Misra et al., 1997; Ormos et al., 1992; Otto et al., 1990; Rothschild, 1992; Sampogna and Honig, 1996; Stern and Khorana, 1989). However, there are also many studies that indicate the direct participation of Arg^{82} in the proton release step, implying that the side chain may be close to the extracellular surface (Balashov et al., 1993; Humphrey et al., 1994; Maeda et al., 1997; Otto et al., 1990). Indeed, the models proposed by Henderson and co-workers placed Arg^{82} down (Arg^{82} (D model), Fig. 1), although the electron density for this residue was not resolved in their study (Grigorieff et al., 1996; Henderson et al., 1990a). The placement of this residue is not resolved by the more recent diffraction studies, all three of which observe electron density for this residue (Kimura et al., 1997a,b; Luecke et al., 1998; Pebay-Peyroula et al., 1997). Whereas the Arg^{82} side chain is down in the structure of Pebay-Peyroula et al. (1997) and up in the structure of Luecke et al. (1998), it is in an intermediate position in the structure proposed by Kimura et al. (1997a,b). (Further refinement of the latter structure (see below) has led to a revised set of coordinates that places Arg^{82} in a location similar to that proposed by Luecke et al. (1998).) The fact that the diffraction studies yield a range of Arg^{82} positions may reflect the flexibility of this residue and a sensitivity to temperature and methods of crystal preparation. As we will examine below, these three models yield very different spectroscopic properties.

In this paper we investigate the possibility that Arg^{82}, rather than Ca(II), serves as the cationic counterion mediating the electrostatic environment of the chromophore in light-adapted bacteriorhodopsin. Because some recent studies predict significant separation of Arg^{82} from the chromophore, however, we also reinvestigate the possibility of a negatively charged binding site. We present a variety of binding site models that differ in terms of local charge and counterion location and compare the ability of these models to rationalize the combined one-photon and two-photon spectroscopic data. We also examine Arg^{82} dynamics to help interpret the recent kinetic studies by Fu et al. (1997) and the possibility that this residue migrates from up to down during the photocycle (Balashov et al., 1993, 1995; Braiman et al., 1988; Dickopf and Heyn, 1997; Rothschild, 1992; Scharnagl et al., 1995).

METHODS

Ground-state calculations on the binding site were carried out by using MM2 molecular mechanics methods (Buckert and Allinger, 1982; Dudek and Ponder, 1995), followed by

MNDO-PM3 all-valence electron semiempirical molecular orbital procedures (Dewar and Thiel, 1977; Dewar et al., 1985; Stewart, 1989; Thiel, 1988). Magnesium was substituted for calcium in all calculations because the PM3 magnesium parameters have been determined with the same rigor as the other parameters (Stewart, 1989), whereas the various calcium parameters available have not been fully tested. This substitution should have no significant impact on our basic conclusions, because both calcium and magnesium are divalent and appear to be identical in terms of impact on the spectroscopic properties of bacteriorhodopsin (see discussion in Stuart et al., 1995).

The advantage of using MM2 as a front-end ("preoptimizer") to the semiempirical MO calculations is both computational speed and access to simulated annealing, which is often essential for avoiding false conformational minima. The implementation of MM2 that we use is commercially available as part of Chem3D Ultra (Version 4.0; CambridgeSoft Corp., Cambridge, MA). This version of MM2 is extended to include a SCF-MO calculation for the π-system atoms. The bond orders from the SCF-MO calculation are used to assign the single- and double-bond torsional force constants within the π-system. This adjustment to the force field is important for describing the conformational flexibility of the protein-bound chromophore, and removal of this adjustment leads to the selection of an incorrect 6-s-*cis* geometry and a higher level of single-bond distortion. Agreement between the MM2 and MNDO-PM3 chromophore geometries is sufficiently good that convergence of the (MM2 preoptimized) MNDO-PM3 geometry optimizations is rapid and direct. Water molecules are also simulated at an acceptable level by the MM2 method, because of the explicit inclusion of the lone-pair orbitals on oxygen and the inclusion of dipole-dipole interactions within the force field. The MM2 calculations included the entire protein, whereas the semiempirical MNDO-PM3 calculations were limited to the residues shown in Fig. 1 (plus Thr^{89}, Pro^{186}, and Trp^{137}). The structure of the chromophore and surrounding binding site was minimized by using, as the starting point, coordinates based on electron cryomicroscopy data provided by Richard Henderson (Grigorieff et al., 1996; Henderson et al., 1990a). We fixed the α-helical backbone atoms in all simulations. After this manuscript was submitted, the coordinates from all three of the recent higher resolution diffraction studies (Kimura et al., 1997b; Luecke et al., 1998; Pebay-Peyroula et al., 1997) became available. These coordinates, with minimization limited to the added hydrogens, the chromophore atoms, and selected water molecules, were also used in a series of calculations to compare the viability of these models with respect to the one-photon and two-photon spectroscopic data.

Excited-state calculations were carried out by using modified neglect of differential overlap with partial single and double configuration interaction (MNDO-PSDCI) molecular orbital theory (Birge et al., 1992a,b; Martin and Birge, 1998; Stuart et al., 1995; Tallent et al., 1992a,b). The CI basis set included all single and all double excitations, including triplet-triplet coupled doubles, from the π-electron system of the chromophore. Our previous MNDO-PSDCI study of the chromophore binding site was based on the PM3 parameterization, because the PM3 parameterization included divalent metals (Stuart et al., 1995). We have carried out the present set of calculations using the standard MNDO-PSDCI parameters, which have been more extensively optimized to reproduce the level ordering and excited-state properties of polyenes and aromatic molecules containing carbon, nitrogen, oxygen, and hydrogen (Martin and Birge, 1998). The MNDO-PSDCI spectroscopic parameters for Mg(II) were obtained by first extrapolating the PM3 parameters using the H, C, N, and O atomic parameters as the comparative atom set, followed by systematic variation until the shifts in charge distributions and transition energies observed in the PM3 calculations were duplicated in the MNDO calculations. The Mg(II) parameters are listed in Table 1. This approach yields parameters that are designed for spectroscopic calculations and should be used for ground-state geometry optimization with caution.

We adjusted the σ- and π-electron mobilities, m, based on the recommendations of Zerner ($m_\sigma = 1.25$, $m_\pi = 0.585$) (Zerner, 1990). This approach improves the ability of

TABLE 1 MNDO-PSDCI parameters for magnesium

Parameter	Value	Description
U_{ss}	−14.40650 eV	s a.o. one-electron one-center integral ($\langle\varphi_s\|H\|\varphi_s\rangle$)
U_{pp}	−13.38050 eV	p a.o. one-electron one-center integral ($\langle\varphi_p\|H\|\varphi_p\rangle$)
β_s	−1.79930 eV	s a.o. one-electron two-center resonance integral term
β_p	−0.78751 eV	p a.o. one-electron two-center resonance integral term
ζ_s	0.64813	s-type slater atomic orbital exponent
ζ_p	1.33180	p-type slater atomic orbital exponent
α	1.34913 eV	atomic core-core repulsion term
G_{ss}	6.61820 eV	s-s a.o. two-electron repulsion integral ($\langle\varphi_s\varphi_s\|r^{-1}\|\varphi_s\varphi_s\rangle$)
G_{pp}	8.24439 eV	p-p a.o. two-electron repulsion integral ($\langle\varphi_p\varphi_p\|r^{-1}\|\varphi_p\varphi_p\rangle$)
G_{sp}	7.90257 eV	s-p a.o. two-electron repulsion integral ($\langle\varphi_s\varphi_s\|r^{-1}\|\varphi_p\varphi_p\rangle$)
G_p^2	6.15828 eV	p-p′ a.o. two-electron repulsion integral ($\langle\varphi_p\varphi_p\|r^{-1}\|\varphi_{p'}\varphi_{p'}\rangle$)
H_{sp}	1.44059 eV	s-p a.o. two-electron exchange integral ($\langle\varphi_s\varphi_p\|r^{-1}\|\varphi_s\varphi_p\rangle$)

These parameters were optimized for MNDO-PSDCI spectroscopic calculations as described in the text. These parameters should be used with caution for ground-state MNDO geometry optimization.

the method to handle longer chain polyenes, where our limitation to single and double CI (rather than full CI) leads to a size inconsistency in describing the relative location of the forbidden and allowed states in longer polyenes (Schulten et al., 1976). We accounted for the resulting overcorrelation of the ground state by multiplying the S_0 correlation energy by one-third before calculating the transition energies (see discussion in Birge et al. (1975), Martin and Birge (1998), and Schulten et al. (1976)).

The two-photon properties of the excited electronic states were calculated by using the summation over states method, as described previously (Birge, 1983; Birge and Pierce, 1979). We included the initial (ground) and final states, as well as the lowest 30 excited singlet states, in the analysis. Test calculations indicate that increasing the basis set to 100 excited states altered the two-photon absorptivity by 2% at most. The relevance of including the initial and final states in the summation was at one time a subject of controversy, but it has now been established that it is not only theoretically correct (Dick and Hohlneicher, 1982; Mortensen and Svendsen, 1981), but also essential for describing accurately the two-photon properties of polar chromophores (Birge et al., 1982; Dick and Hohlneicher, 1982) and protein-bound chromophores (Birge and Zhang, 1990). Our calculations assumed a damping constant of 0.5 eV, which prevents fortuitous resonances from unrealistically enhancing the two-photon absorptivity. We adopted the experimental maximum value of the frequency-normalized line-shape function ($g_{max} = 8.828 \times 10^{-15}$ s; Birge and Zhang, 1990).

Calculation of error

The quality of the binding site model is quantitatively assigned by using the following weighted error factor, ϵ_w:

$$\epsilon_w[V_{calc}, V_{obsvd}, V_{error}] = \left(\frac{(V_{calc} - V_{obsvd})^2}{V_{obsvd}^2 + V_{error}^2}\right)^{1/2} (1 - 2^{-(V_{calc}-V_{obsvd})^2/V_{error}^2}) \quad (1)$$

where V_{calc} is the calculated value, V_{obsvd} is the experimentally observed value, and V_{error} is the experimental error. This function returns a dimensionless error factor that is weighted by the experimental error, assuming a Gaussian error distribution (Stuart et al., 1995). The key advantage of using this function is that the error factor that is returned is independent of the choice of units and is scaled to provide a statistically relevant value. When there is no experimental error, the function simply returns the absolute value of the error divided by the observed value (i.e., $\epsilon_w = |(V_{calc} - V_{obsvd})V_{obsvd}^{-1}|$). If the error in the calculation is equal to the experimental error, we get

$$\epsilon_w = \frac{|V_{calc} - V_{obsvd}|}{2\sqrt{V_{error}^2 + V_{obsvd}^2}} \quad (\text{if } V_{error} = |V_{calc} - V_{obsvd}|) \quad (2)$$

In this case, the error factor returns a value that equals the absolute error divided by twice the root mean square of the error and the observed value. The experimental error is normally much smaller than the experimental value, and in such instances the above condition generates a value of ϵ_w roughly half that of the "standard" error. However, as the experimental error approaches the observed value, the factor is reduced further by $1/\sqrt{2}$. Finally, we note that if the calculated value is identical to the observed value, $\epsilon_w = 0$, regardless of the experimental error.

The ϵ_w function is used to assign an error factor for each of four key parameters, the transition energy (ΔE), the one-photon oscillator strength (f), the two-photon absorptivity (δ), and the ratio of the two-photon absorptivities ($\delta(S_1)/\delta(S_2)$). The total error for the one-photon data is calculated as the sum of the errors in the transition energies and oscillator strengths into the first two excited singlet states:

$$\epsilon_{one\text{-}photon} = \tfrac{1}{4}(\epsilon_w[\Delta E(S_1)] + \epsilon_w[f(S_1)] + \epsilon_w[\Delta E(S_2)] + \epsilon_w[f(S_2)]) \quad (3)$$

where we have simplified the notation by replacing $\epsilon_w[\Delta E_{calc}, \Delta E_{obsvd}, \Delta E_{error}]$ with $\epsilon_w[\Delta E]$ and used comparable simplifications for the oscillator strength. Similarly, the total error for the two-photon data is calculated as the sum of the errors in the two-photon absorptivities and the ratio of the two-photon absorptivities of the first two excited singlet states:

$$\epsilon_{two\text{-}photon} = \frac{1}{3}\left(\epsilon_w[\delta(S_1)] + \epsilon_w[\delta(S_2)] + \epsilon_w\left[\frac{\delta(S_1)}{\delta(S_2)}\right]\right) \quad (4)$$

In our previous study (Stuart et al., 1995) we included the change in dipole moment in the excited state, but we have since concluded that this represents an overemphasis on this particular component, because the nonlinear properties of the low-lying excited states of bacteriorhodopsin are dominated by initial and final state properties (Birge and Zhang, 1990; Yamazaki et al., 1998). Instead, we have included the ratio of the two-photon absorptivities, which is dominated by the proper assignment of both the dipolar and electronic properties of the two lowest-lying singlet states. The total error for a given model is then calculated as the sum of all of the individual component errors divided by the total number of measurements:

$$\epsilon_{total} = \tfrac{1}{7}(4\epsilon_{one\text{-}photon} + 3\epsilon_{two\text{-}photon}) \quad (5)$$

Higher excited states, such as the "$^1A_g{}^{*+}$" state, were not included in our error analyses because of the uncertainty in assigning the location and two-photon properties of these states.

RESULTS

We carried out a series of model compound studies based on highly simplified versions of the binding site as well as more complete models including the amino acid residues

shown in Fig. 1. The model compound studies provide a useful perspective of which elements of a more global model are important in defining the spectroscopic properties of the chromophore. It is often difficult to determine the origin of the electronic shifts that correspond to the larger binding site models, because the inclusion of the full surrounding amino acid environment produces a host of more subtle interactions that are too numerous and interdependent to characterize.

Model compound studies

Our preliminary set of calculations was carried out on simple, minimalized models of the chromophore binding site. The Schiff base chromophore and the lysine side chain were included, and the chromophore was locked into a planar all-*trans*, 6-s-*trans* geometry. Aspartic acid side chains were simulated using CH_3-COO^- groups, the Arg^{82} side chain by NH_4^+, and the divalent metal cation using Mg^{2+}. The model binding sites studied are labeled A–J (shown at the top of Fig. 3); they represent a series of neutral and charged binding sites made up of various combinations of the chromophore, water, and positively or negatively charged counterions. We limited our study to neutral and singly charged (0, $\pm$1) sites. In each case, the geometry was optimized with fixed intramolecular hydrogen bond lengths or metal-to-oxygen separations of 1.8 Å (*dashed lines* in Fig. 3). These constraints were necessary to prevent the geometry optimization process from generating more stable but less relevant models. For example, free minimization of model E leaves one of the CH_3-COO^- groups to interact with the imine hydrogen (as shown in *C*) but moves the other CH_3-COO^- group above the chromophore to interact with the hydrogen atoms on the δ-carbon of lysine and the C_{13} atom of the chromophore. Such a geometry, while interesting, is not relevant to an investigation of the bR binding site. The calculated linear and nonlinear optical properties of these sites are listed in Table 2 and graphed in Fig. 3.

By reference to Table 2, we see that the total error factor for the various model compounds ranges from 0.085 (model D, a neutral binding site with a single ASP residue mediated via water) to 0.603 (an isolated protonated Schiff base). We note that model D is quite similar to our original model of the binding site (Birge and Zhang, 1990), proposed before the availability of the diffraction study of Henderson, showing two Asp residues in the binding site (Henderson et al., 1990a).

Full binding site studies

We generated a series of binding site models by using the protein coordinates provided to us by Richard Henderson, based on his recent optimization of the diffraction data (Grigorieff et al., 1996) as well as models created by using the distance information provided in the more recent, higher resolution diffraction studies (Kimura et al., 1997a,b; Luecke et al., 1998; Pebay-Peyroula et al., 1997). Hydrogen atoms were added by using automatic rectification methods inherent in Chem3D, followed by MM2 energy minimization of the hydrogen atoms, with all other atoms held fixed. The binding site residues that were included in the MNDO-PM3 calculations are shown in Fig. 1, but the entire protein was included in the MM2 geometry optimizations. When the more recent diffraction studies were modeled, we used the coordinates provided by Henderson et al. (Grigorieff et al., 1996) as the starting point and introduced the published distance data from the other diffraction studies as constraints. Water molecules were added and optimized until the MNDO-PM3 heat of formation no longer decreased based on a bulk water energy comparison. That is, if moving a water molecule from the bulk phase to the binding site lowered the energy of the supermolecular system, the water molecule was included in the binding site. We simulated bulk water by using 48 water molecules and removing water from the center, followed by reminimization. Water was first minimized by using the MM2 method, but usually moved significantly when the MNDO-PM3 calculation was carried out. Simulated annealing was performed to verify a true energy minimum for the water molecules. In some cases, we added excess water molecules to stabilize otherwise unstable conformations (see below).

We examined eight different negative binding sites characterized by a positively charged chromophore and two negatively charged Asp residues (Asp^{85} and Asp^{212}). The negatively charged binding sites are labeled N#; the two best results are listed in Table 2, and the best (N2) is shown schematically in Fig. 4. The negatively charged sites failed uniformly to match experiment, and all yielded errors greater than 0.77. Only two (N1 and N2) had errors below 1.0, and both of these were characterized by having water directly associated with the imine proton and forming hydrogen bonds to Asp^{85} and Asp^{212}. These two models were all relatively high in energy when compared to the neutral and positively charged sites. Thus the negatively charged sites are poor candidates in terms of both experimental agreement (Table 2) and theoretical prediction.

We investigated only one new binding site model involving calcium, having carried out an extensive study of six such models during our previous investigation (Stuart et al., 1995). All six models gave errors lower then 0.45, significantly better than the negative site error distribution. The two best in terms of calculated energy and agreement with experiment, P1 and P2, are shown in Fig. 2, and correspond to models B and A, respectively, of Stuart et al. (1995). Model P3 is also shown in Fig. 2 and is based on the superconducting quantum interference device magnetometry and ab initio molecular orbital studies of Pardo et al. (1998). This latter study places a divalent metal atom within the chromophore binding site equidistant (~2 Å) from the four carboxylate oxygen atoms of Asp^{85} and Asp^{212} (see figure 5 of Pardo et al., 1998).

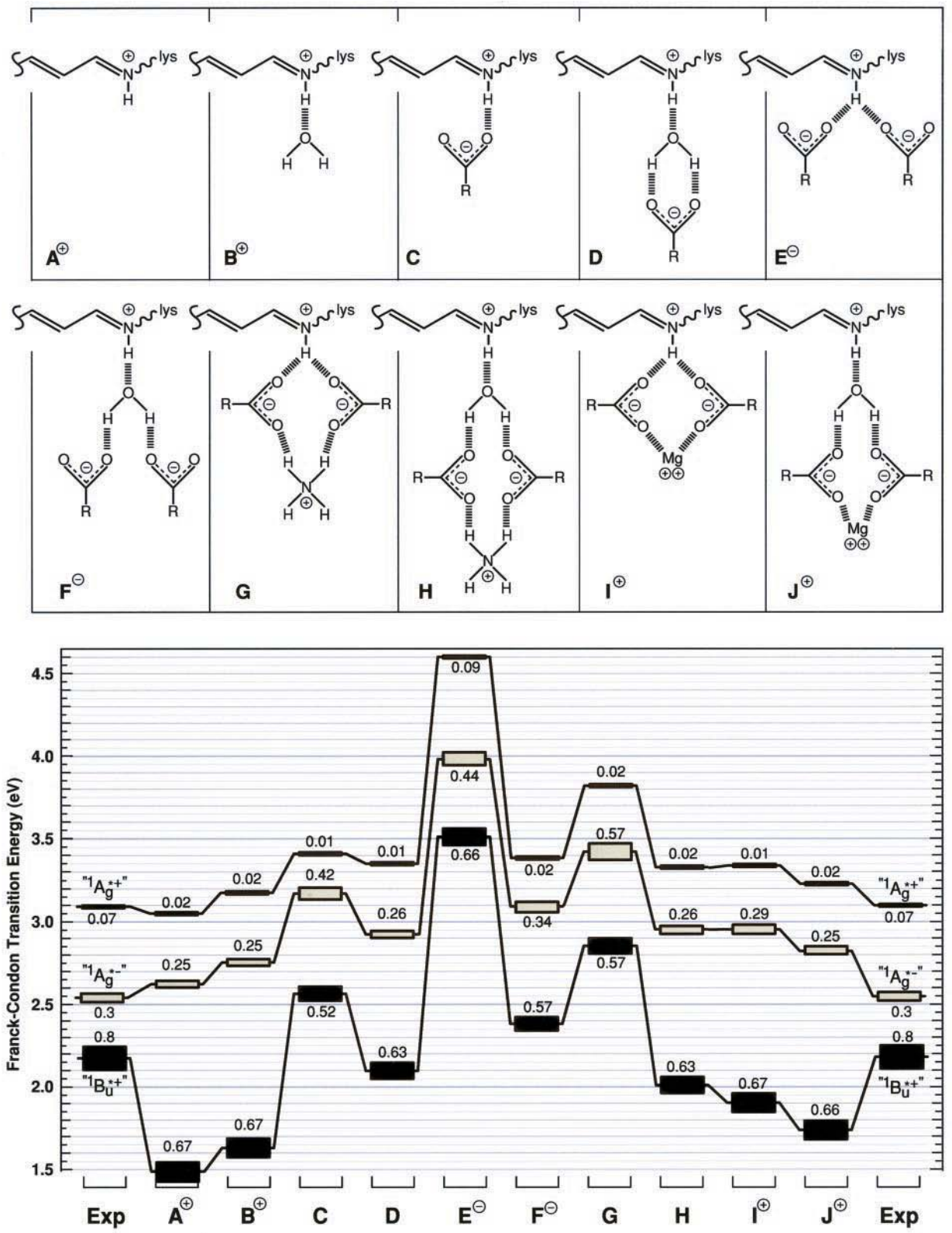

FIGURE 3 A comparison of the one-photon properties of the 10 binding site models, A–J, schematically shown in the top insets.

Our previous study of bR binding sites included only one model of a binding site in which Arg^{82} was moved up into the binding site (Stuart et al., 1995). This model was based on the recommendations of Bashford and Gerwert (1992); it placed the Arg^{82} side chain at a distance of 7.5 Å from the Schiff base nitrogen. This geometry is unstable to MNDO-

TABLE 2 Analysis of error in the calculated one-photon and two-photon properties

Model	$\Delta E(S_1)$ (eV)	$f(S_1)$	$\Delta E(S_2)$ (eV)	$f(S_2)$	One-photon error	$\delta(S_1)$ GM/10^2	$\delta(S_2)$ GM/10^2	$\delta(S_1)/\delta(S_2)$	Two-photon error	Wtd. total error
Exp	2.17	0.8	2.54	0.3		2.9	1.2	2.4		
Exp err	0.01	0.07	0.1	0.15		0.5	0.9	1.0		
A	1.463	0.673	2.613	0.252	0.122	12.50	105.60	0.12	1.25	0.603
B	1.622	0.665	2.750	0.247	0.125	11.53	34.41	0.34	1.23	0.599
C	2.561	0.516	3.173	0.419	0.227	0.79	0.40	1.96	0.49	0.341
D	2.103	0.632	3.008	0.259	0.107	2.78	1.06	2.61	0.06	0.085
E	3.505	0.661	3.989	0.437	0.382	4.27	1.66	2.57	0.18	0.294
E	2.376	0.572	3.089	0.335	0.150	15.75	5.61	2.81	0.56	0.325
G	2.855	0.571	3.427	0.574	0.421	2.05	0.81	2.53	0.18	0.318
H	2.020	0.634	2.963	0.257	0.111	1.52	0.70	2.19	0.28	0.186
I	1.902	0.665	2.949	0.294	0.110	10.74	1.53	7.01	0.50	0.276
J	1.744	0.658	2.829	0.246	0.123	11.44	6.56	1.74	0.58	0.320
P1	2.183	0.664	3.122	0.260	0.099	5.68	0.26	22.28	0.70	0.356
P2	1.733	0.657	2.804	0.252	0.121	9.77	6.42	1.52	0.60	0.324
P3	1.626	0.666	2.724	0.257	0.119	13.28	19.93	0.67	1.23	0.597
N1	2.878	0.298	3.377	0.778	0.676	1.99	3.92	0.51	0.97	0.804
N2	2.791	0.367	3.312	0.664	0.549	5.17	6.59	0.78	1.06	0.769
U1	2.453	0.717	3.120	0.342	0.107	1.91	0.58	3.29	0.32	0.199
U2	2.364	0.805	3.497	0.326	0.117	3.21	0.30	10.74	0.52	0.289
U3	2.438	0.721	3.074	0.338	0.099	2.15	0.27	7.87	0.54	0.289
U4	2.461	0.620	2.978	0.412	0.159	0.81	0.54	1.50	0.51	0.307
1AP9*	2.377	0.585	3.073	0.555	0.308	1.05	0.33	3.19	0.50	0.389
1AT9#	2.679	0.659	3.459	0.541	0.340	1.51	0.65	2.33	0.29	0.317
1BRX§	2.703	0.619	3.570	0.433	0.260	3.09	1.04	2.98	0.10	0.190

Models A–J are shown in Fig. 3; P1, P2, and P3 in Fig. 2; N2 in Fig. 4; U1 in Fig. 5; U2 in Fig. 6; and 1AP9, 1AT9, and 1BRX in Fig. 8. The variables that appear in columns 2–11 are defined in Eqs. 3–5 and associated text. GM, Göppert-Mayer two-photon absorptivity unit (1×10^{-50} cm^4 s molecule^{-1} photon^{-1}).

*PDB ID for the 2.5-Å structure obtained from Pebay-Peyroula et al. (1997) (see text).

#PDB ID for the 2.8-Å structure based on a refinement of the structure originally reported by Kimura et al. (1997b) (see text).

§File name for the 2.3-Å structure kindly provided to us by Drs. Lanyi and Luecke and based on their study (Luecke et al., 1998) (see text).

PM3 optimization (see, also, the recent study of Nagel et al., 1997). However, when locked into this position, the site yielded reasonable agreement with experiment but was not as successful as the metal cation-mediated sites shown in Fig. 2. As discussed above, we were prompted to reinvestigate the potential role of Arg^{82} as a counterion, and we studied a total of 12 U sites, where the "U" label refers to Arg^{82} up. The two best based on minimization of the Henderson coordinates are listed in Table 2 as U1 and U2 and are shown in Figs. 5 and 6. We have learned that the apparent failure of our previous Arg^{82} counterion model was due to a failure to properly hydrate the model (see Discussion). The Arg^{82} "up" models are the most successful models based on the error analysis (Table 2).

We also carried out calculations using the coordinates from three of the recent higher resolution diffraction studies (Kimura et al., 1997b; Luecke et al., 1998; Pebay-Peyroula et al., 1997). These results are listed at the bottom of Table 2 by reference to the PDB ID (or coordinate file names), where 1AP9 is for the 2.5-Å structure from Pebay-Peyroula et al. (1997), 1AT9 is for the 2.8-Å structure from Kimura et al. (1997b), and 1BRX is for the 2.3-Å structure kindly provided to us by Drs. Lanyi and Luecke and based on their study (Luecke et al., 1998). As of this writing, only the first two structures were available on the Brookhaven Protein Data Bank server. Hydrogen atoms were added by using Quanta (MSI) and were minimized by using an MM2 force field. Subsequently, the entire chromophore was minimized by using MNDO-PM3 semiempirical molecular orbital theory. Waters were added when necessary to improve the fit to experiment. A more detailed explanation of our methods is reserved for the Discussion.

DISCUSSION

Our goal in this paper is to provide a realistic model of the chromophore binding site in light-adapted bacteriorhodopsin (bR). We presented above the results of calculations for a range of models that can be divided into three groups with respect to charge (negatively charged: E, F, N1, and N2; positively charged: A, B, I, J, P1, P2, and P3; neutral: C, D, G, H, U1-U4, 1AP9, 1AT9, and 1BRX). However, some of the "neutral" systems have Arg^{82} down, yielding a site that

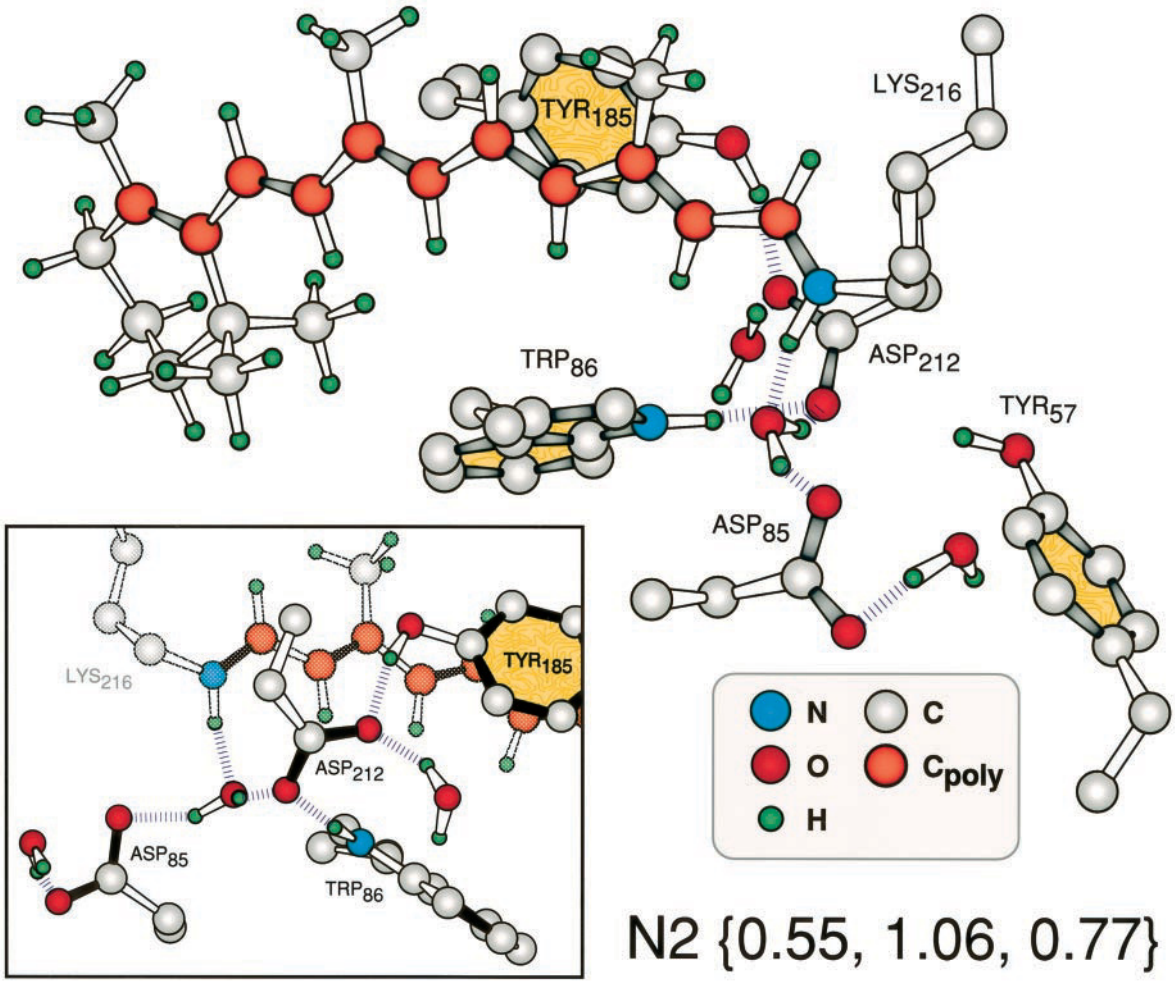

FIGURE 4 The negative binding site model yielding the best agreement with experiment (N2, Table 2) is characterized by a strong interaction of water with the Schiff base imine proton, which mediates the interaction of Asp^{85} and Asp^{212} with the protonated Schiff base (see *inset at lower left*). The numbers in curly braces are as follows: $\{\epsilon_{\text{one-photon}}, \epsilon_{\text{two-photon}}, \epsilon_{\text{total}}\}$, with all data taken from Table 2. We exclude this and all other negatively charged binding sites as unrealistic models of light-adapted bacteriorhodopsin.

has spectroscopic properties closer to a negatively charged site. As a starting point, it is useful to reiterate the observations of our original study of the two-photon properties of bacteriorhodopsin (Birge and Zhang, 1990) and determine whether any of these observations are contradicted by the present study. The four observations were 1) the chromophore is protonated, 2) the binding site is very ionic and may be charged, 3) there are no bare charges near the β-ionylidene ring, and 4) at least one water molecule interacts strongly with the imine proton of the chromophore (Birge and Zhang, 1990). The best model predicted a neutral binding site with a water molecule hydrogen bonded to the protonated Schiff base imine proton and a single negative counterion, Asp^{212} (Birge and Zhang, 1990). It is sufficient to note that our calculations, taken by themselves, still support all of these observations. Indeed, the best model based on error analysis is D, which is a single Asp residue interacting directly with the imine proton through water (Fig. 3). This model is, of course, wrong, because subsequent studies have shown that there are two negative Asp residues in the binding site (Grigorieff et al., 1996; Henderson et al., 1990a; Kimura et al., 1997b; Luecke et al., 1998; Pebay-Peyroula et al., 1997). We can conclude, however, that the current set of calculations fully supports observations 1, 3, and 4. The chromophore is protonated and the diffraction studies have uncovered no charged amino acids residues near the ring (Luecke et al., 1998; Pebay-Peyroula et al., 1997). However, only one study identified a water molecule in direct contact with the imine proton of the chromophore (Luecke et al., 1998). Our suggestion that the binding site may be charged, however, is problematic. We will first examine the results of our model compound studies. We will then examine the full binding site models.

Model compound studies indicate the importance of hydration

We were surprised to find that many of the simple model compounds (A–J) generated small one-photon and/or two-

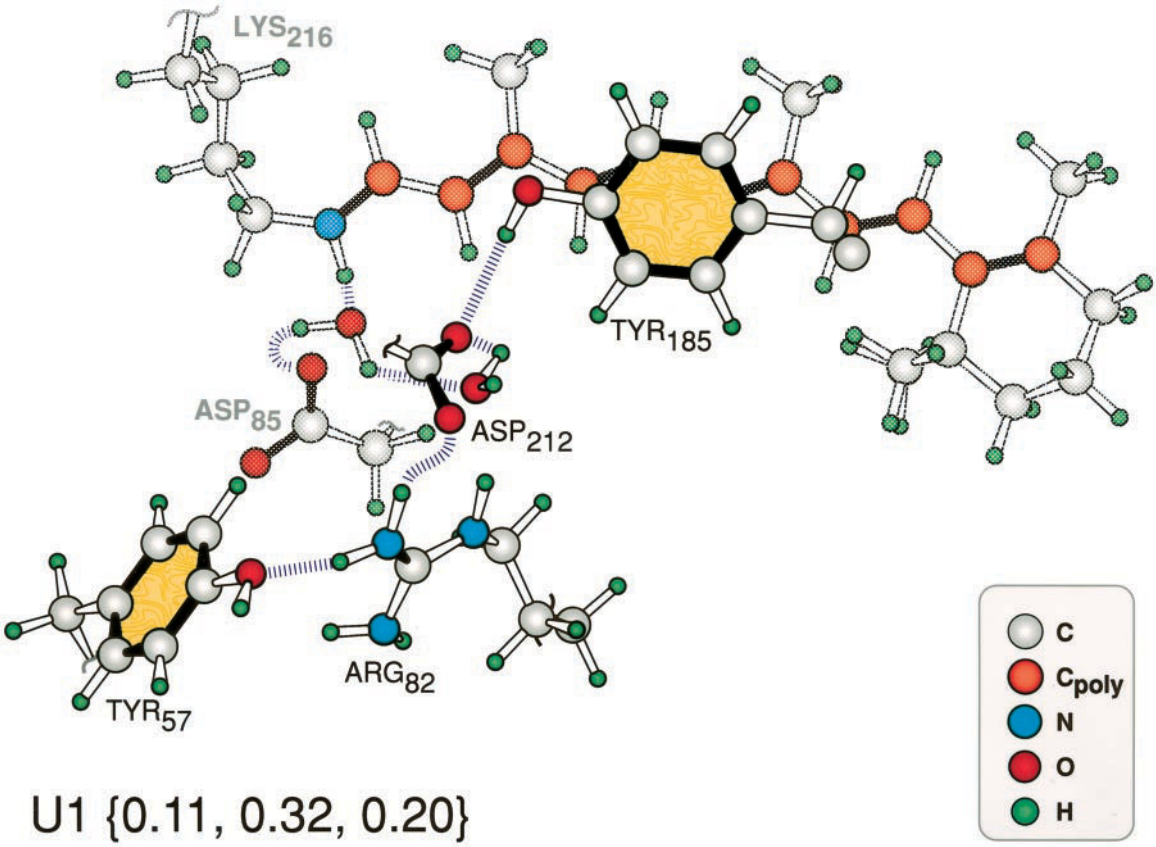

FIGURE 5 The U1 model, a neutral binding site characterized by an Arg^{82}–Schiff base nitrogen distance of 5.6 Å. In this model, Asp^{85} is the primary counterion to the protonated Schiff base chromophore and Arg^{82} and Asp^{212} form a salt bridge, with secondary stabilization from Tyr^{185} and Tyr^{57}. Three water molecules were included in the simulation, but only two are visible in this figure. Error values from Table 2 are given in curly braces: $\{\epsilon_{\text{one-photon}}, \epsilon_{\text{two-photon}}, \epsilon_{\text{total}}\}$. Note that this binding site model has the second lowest heat of formation and yields the best agreement with the two-photon data.

photon errors. The excellent agreement with experiment is, however, fortuitous. But these studies do provide an interesting perspective on what components are important for satisfying the linear and nonlinear optical data. First, we note that the two best models are neutral (D and H). Second, we note that these two models are also characterized by the direct association of water with the imine proton, thereby mediating the interaction of the charged Asp residues with the chromophore. These calculations provide evidence that water mediation of the chromophore-protein interaction is an important component in a binding site model, an observation that will be supported in greater substance below. These calculations also support the notion of a neutral protein binding site, but such an observation is premature, given the simplicity of these model compound studies.

Negatively charged sites are spectroscopically unrealistic

We know from previous studies that the Schiff base chromophore is protonated and that Asp^{85} and Asp^{212} are both unprotonated in bR (Eyring and Mathies, 1979; Metz et al., 1992). Thus, in the absence of a (positively charged) counterion, the binding site is negatively charged, as supported by the early models of Henderson and co-workers (Grigorieff et al., 1996; Henderson et al., 1990a,b) and the more recent diffraction study of Pebay-Peyroula et al. (1997). We investigated eight different negative binding sites; the best model (N2) is shown in Fig. 4. The two best models studied (N1 and N2) produce unacceptable errors in both the calculated one-photon and two-photon properties (Table 2). The most important observation is that all of the negatively charged sites involving the full binding site (residues in Fig. 1) produce a lowest-lying "$^1A_g{}^{*-}$" state, which is contrary to experimental observation (Birge and Zhang, 1990). We are confident that the binding site of light-adapted bacteriorhodopsin is not negatively charged.

Positively charged sites cannot be ruled out spectroscopically

The only positively charged binding site models investigated here have a divalent metal cation in what we have termed the chromophore-adjacent cation binding site. The two best models are shown in Fig. 2, and their properties have been discussed in detail previously (Stuart et al., 1995). As can be seen by reference to Table 2, the MNDO-PSDCI calculations based on these two models reproduce

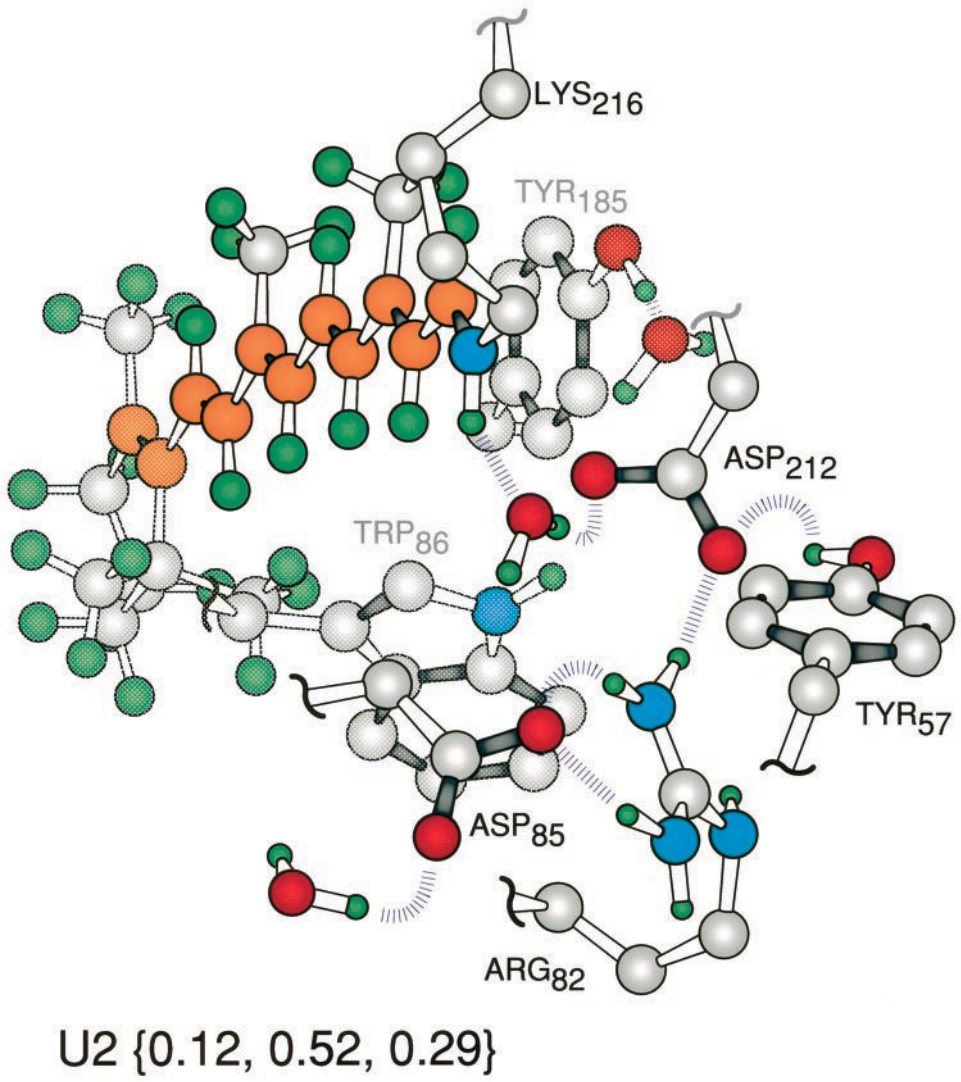

FIGURE 6 The U2 model, a neutral binding site characterized by an Arg^{82}–Schiff base nitrogen distance of 5.3 Å. In this model, Asp^{212} is the primary counterion to the protonated Schiff base chromophore, and Arg^{82} and Asp^{85} form a salt bridge. Error values from Table 2 are given in curly braces: $\{\epsilon_{\text{one-photon}}, \epsilon_{\text{two-photon}}, \epsilon_{\text{total}}\}$. This model is slightly higher in energy than U1 but is a metastable conformational product of dynamic simulations.

the one-photon data very well and reproduce the two-photon data with reasonable accuracy. Furthermore, the recent magnetometry study of Pardo et al. (1998) provides support for a chromophore-adjacent cation binding site. In that regard, we included a calculation based on the optimized geometry proposed by these investigators (P3 is based on figure 5 from Pardo et al., 1998). Our concern about the viability of these models is not due to a failure to accommodate the one-photon and two-photon spectroscopic data, but rather to selected recent diffraction and kinetic studies (Fu et al., 1997; Kimura et al., 1997b; Luecke et al., 1998). We therefore turn to a detailed examination of neutral chromophore binding sites in which Arg^{82} serves as the single positively charged counterion.

Neutral sites mediated via Arg^{82} are the most realistic

We have found three classes of neutral binding sites that provide satisfactory agreement with the one-photon and two-photon spectroscopic data and one model that provides excellent agreement with experiment. These binding sites, labeled U1 and U2, are shown, respectively, in Figs. 5 and 6. In U1 (Fig. 5), Asp^{85} is the primary counterion to the protonated Schiff base chromophore, and Arg^{82} and Asp^{212} form a salt bridge, with secondary stabilization from Tyr^{185} and Tyr^{57}. This model is in close agreement with the recent diffraction study of Luecke et al. (1998). In U2 (Fig. 6), Asp^{212} is the primary counterion to the protonated Schiff base chromophore, and Arg^{82} and Asp^{85} form a salt bridge. Although U1 is lower in energy than U2, these two sites differ by only 12 kJ mol^{-1} and should be viewed as equivalent energetically because of the experimental error inherent in our semiempirical procedures. It is possible that both of these conformers could be populated at ambient temperature and exist in equilibrium. Two other models that we examined, U3 and U4, were generated by applying distance constraints based on the reported electron diffraction cryomicroscopy study of Kimura et al. (1997b). The published geometry placed Arg^{82} in an intermediate position that was unstable in our simulations. To achieve a metastable structure it was necessary to add nine water molecules in the

cavity surrounded by Tyr^{57}, Arg^{82}, Asp^{85}, Trp^{86}, Asp^{212}, and the chromophore. Minimization yielded U3 (not shown). The large number of correlated water molecules transfer the positive charge on Arg^{82} into the Asp^{85}:Asp^{212} region and generate a spectroscopically viable model. However, the number of water molecules required to create a metastable geometry exceeds by nearly two the number likely to be present in this region (see discussions in Edholm et al., 1995; Luecke et al., 1998; Pebay-Peyroula et al., 1997; Sampogna and Honig, 1996). Thus we also carried out a calculation in which we removed all but three equilibrated water molecules between Arg^{82} and the chromophore. The resulting model, U4, is not shown, but the calculated spectroscopic properties are summarized in Table 2. This model is not stable, as it rapidly decays ($\Delta t < 100$ ps) to form U1 or U2 (see below) and is even less successful at accommodating the spectroscopic data (Table 2). Since this publication, however, Kimura and co-workers have refined their model, and the resulting coordinates have much in common with the model proposed by Luecke et al. (1998). The very recent release of the coordinates from all three high-resolution diffraction studies allows us a much better perspective on the spectroscopic consequences associated with the actual structures. We examine all three in the following section.

Comparison of the high-resolution diffraction models

The three recent high-resolution (<3 Å) diffraction models differ significantly with to the position of the key electrostatic residues (Arg^{82}, Asp^{85}, and Asp^{212}) relative to the chromophore, as shown in Fig. 7. As one might anticipate, these three structures yield very different one-photon and two-photon calculated properties. However, a meaningful comparison among the three structures based on the PDB files is not possible. First, these files do not contain hydrogen atoms, whereas the all-valence electron MNDO-PSDCI semiempirical molecular orbital procedures require these atoms. Thus hydrogen atoms were added by using Quanta (MSI) and were minimized by using an MM2 force field. During this process, all other atoms were held fixed. Subsequently, the entire chromophore was minimized by using

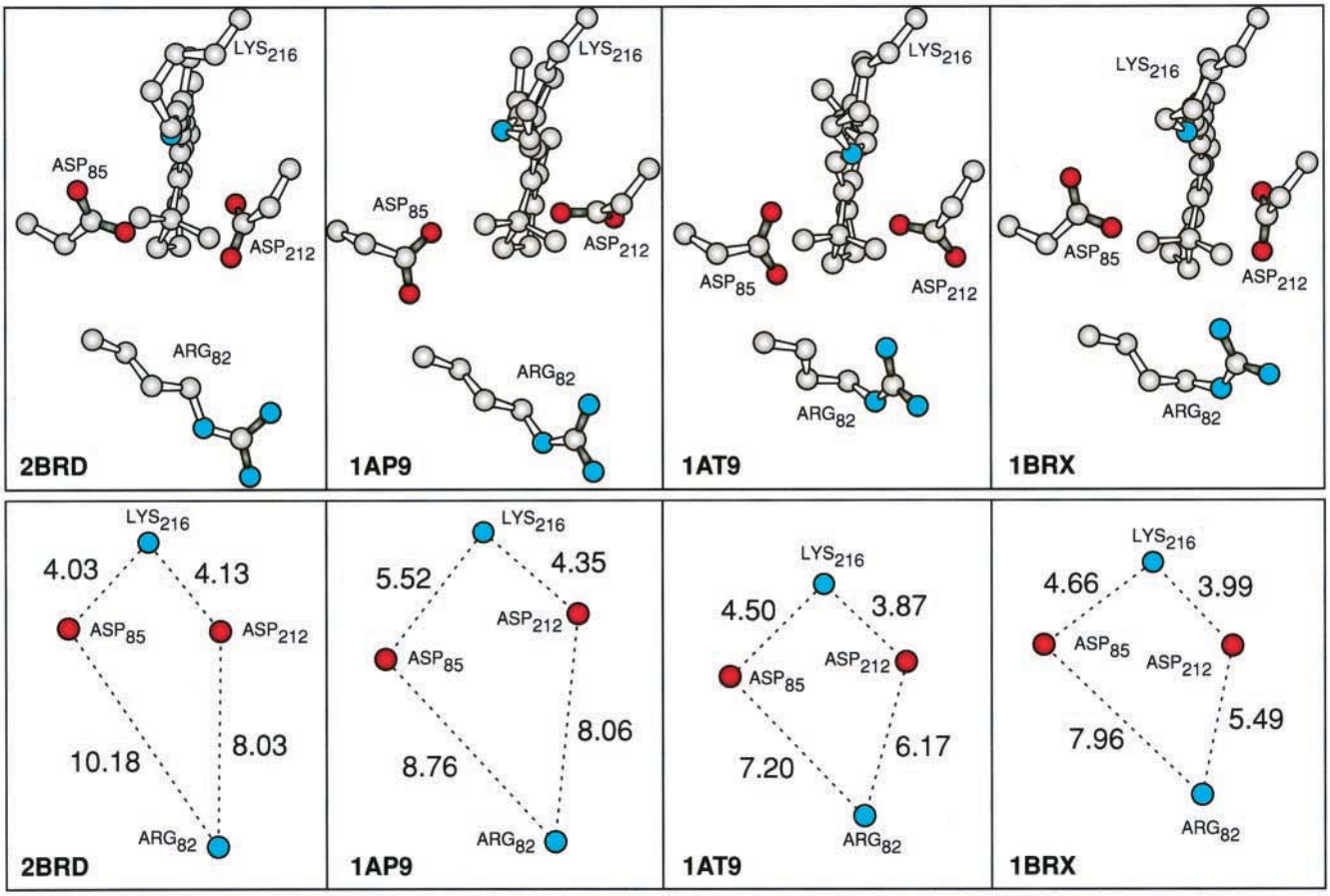

FIGURE 7 A comparison of the location of Arg^{82} relative to Asp^{85}, Asp^{212}, and the chromophore in the four diffraction-based models of light-adapted bacteriorhodopsin. The labels refer to the PDB ID (or file names): 2BRD (Grigorieff et al., 1996), 1AP9 (Pebay-Peyroula et al., 1997), 1AT9 (refined structure based on that by Kimura et al. (1997b)), and 1BRX (Luecke et al., 1998). The single spheres in the lower set show the location of the charge centroids (*blue* is positive, *red* is negative) and the dashed lines indicate separations, which are labeled in Ångstroms.

MNDO-PM3 semiempirical molecular orbital theory, while holding all other atoms fixed. Finally, all of the hydrogen atoms were minimized along with the chromophore to yield the final (nonaqueous) geometry. In some cases, additional water molecules were added to the binding sites and minimized via PM3 procedures (see below). The chromophore minimization process might seem unnecessary, and indeed, it had little impact on our calculations for the 1AP9 and 1BRX structures. In contrast, the chromophore geometry proposed in the 1AT9 study is so highly distorted that the calculated electronic transitions are blue shifted such that the lowest-lying allowed singlet state is predicted at 232 nm ($f = 0.460$). (The authors note in the remarks of the PDB file that further refinement of the chromophore is required.) Our goal in this process was to neutralize to the extent possible differences among the three models due to water placement and chromophore geometry, so that the position of the other residues dominated the agreement or lack of agreement with experiment. The final geometries of the key residues and nearby water molecules are shown in Fig. 8. Note that the lightly colored water molecules were added, or moved, in our search. Only in the case of the structure by Luecke et al. (1998) (1BRX) were the waters as listed in the PDB file in a near-optimal location with respect to calculated error (rightmost column in Table 3).

A comparison of the three models indicates that the structure of Luecke et al. (1998), 1BRX, provides the best agreement with experiment; the refined structure of Kimura et al. (1997), 1AT9 shows relatively poor agreement with experiment; and the structure of Pebay-Peyroula et al. (1997), 1AP9, is even worse (Table 2). We note that the total error (Table 2) calculated for the latter two structures is worse when the water is removed from the binding site. The problem with the model of Pebay-Peyroula et al. (1997) is associated with the effective charge on the binding site. Because Arg^{82} is separated significantly from the Asp^{85} and Asp^{212} residues, the chromophore environment approaches a negatively charged binding site, and this causes a near-reversal of the two lowest-lying excited states, as was observed for N1 and N2. If the model of Pebay-Peyroula et al. (1997) is correct, then a strong case can be made for a divalent cation inside the binding site (Fig. 2 and related discussion). The problem with the structure of Kimura et al. (1997) is more difficult to determine, because the relative positions of the charged residues near the chromophore in 1AT9 are similar to those in the structure of Luecke et al. (1998), 1BRX (see Fig. 7). It is sufficient to note for the present study that the location of Arg^{82} is critical, but it is not the only critical determinant of the one-photon and two-photon spectroscopic properties. The location and orientation of the Arg^{82}, Asp^{82}, and Asp^{212} residues can have a major impact on the electronic properties in subtle ways that are difficult to quantify. We note further that the MNDO/PM3 heat of formation calculated for the 1AT9 binding site was significantly higher than that calculated for 1AP9 and 1BRX.

We close this section with a brief discussion of the role of water in mediating the properties of the three binding site models. First, the agreement with experiment improves for all models when a water molecule is directly hydrogen-bonded to the imine proton. Such a water molecule is found in the structure of Luecke et al. (1998), 1BRX, but is absent from the other two structures. This absence is not surprising when the 1AT9 model is examined, because no water molecules were identified at all. However, the model of Pebay-Peyroula et al. (1997), 1AP9, includes the explicit assignment of 26 water molecules, but none are closer than 6.7 Å to the Schiff base nitrogen. Our semiempirical MNDO-PM3

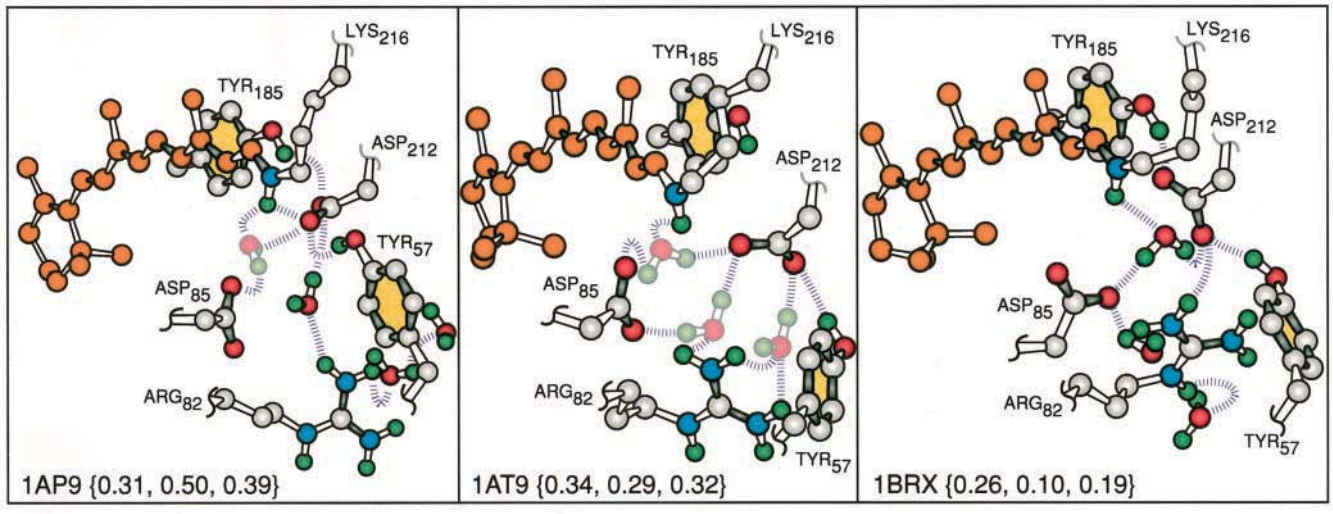

FIGURE 8 A comparison of the key binding site residues that mediate the electrostatic properties of the chromophore in the three recent diffraction models: 1AP9 (Pebay-Peyroula et al., 1997), 1AT9 (refined structure based on that by Kimura et al. (1997b)), and 1BRX (Luecke et al., 1998). In all cases, the chromophore has been minimized by using MNDO/PM3 semiempirical molecular orbital theory, and if additional water molecules improved agreement with experiment, these additional water molecules are shown in lighter colors (one water molecule was added to 1AP9 and three water molecules to 1AT9). Error values from Table 2 are given in curly braces: $\{\epsilon_{\text{one-photon}}, \epsilon_{\text{two-photon}}, \epsilon_{\text{total}}\}$.

TABLE 3 Spectroscopic properties of selected site-directed mutants of bacteriorhodopsin

Mutant and expression system*		λ^{LA}_{max} (nm) [pH]#	λ^{DA}_{max} (nm) [pH]§	Ref.¶
ebR‖**	E	560 [7.3], 561 [6]	550 [7.3], 551 [6]	(a–c)
R82A	E	—	547 [7.3]	(a)
R82Q##	E	553 [8], 580 [6]	548 [8], 547 [7.3], 575 [6]	(a–d)
R82D/D85R§§	E	592 [6]	597 [6]	(c)
R82Q/D212N¶¶	E	568 [6]	562 [6]	(c)
R82Q/D85N‖‖	E	583 [6]	582 [6]	(c)
WT	S	568 [7.8, 6.5, 4], 606 [2]	558 [7.8, 6.5, 4], 597 [2]	(e)
WT (deion)	S	—	606 [4]	(e)
D85N***	S	616 [7.8, 6.5], 606 [4], 596 [2]	—	(e)
D85N (deion)	S	596 [4]	—	(e)
R82Q/D85N	S	586 [7.8, 6.5], 576 [4], 576 [2]	—	(e)
R82Q/D85N (deion)	S	576 [4]	—	(e)
D212N###	S	586 [7.8], 576 [6.5], 558 [4], 586 [2]	—	(e)
D212N (deion)	S	536 [4]	—	(e)
Y185F§§§ ¶¶¶	S	—	556 [7.8, 6.5], 574 [4], 590 [2]	(e)
Y185F (deion)¶¶¶	S	—	590 [4]	(e)
R82Q/Y185F¶¶¶	S	—	578 [7.8, 6.5], 574 [4], 568 [2]	(e)
R82Q/Y185F (deion)¶¶¶	S	—	568 [4]	(e)
R82K	S	—	552 [6.5], 611 [2.2], 590 [1.1]	(f)
R82A	S	601 [<5], 565 [8.8], 555 [>9]	574 [2], 587 [4], 585 [6], 555 [8.8]	(g, h)
R82Q	S	553 [>9]	587 [6]	(h, i)

*Mutants are listed by letter abbreviations: native residue number replacement residue. The expression system (organism) is either *E. coli* (E) or *H. salinarium* (S).

#Absorption maximum of the light-adapted protein (nm) at a given pH listed in brackets. Note that many mutants do not fully light-adapt to generate pure all-*trans* chromophore.

§Absorption maximum of the dark-adapted protein (nm) at a given pH listed in brackets.

¶References: (a) Otto et al. (1990). (b) Stern and Khorana (1989). (c) Marti et al. (1991). (d) Duñach et al. (1990b). (e) Zhang et al. (1993). (f) Balashov et al. (1995). (g) Balashov et al. (1993). (h) Brown et al. (1993). (i) Renthal et al. (1997).

‖Mutants expressed in *E. coli* generate a monomeric protein, with a characteristic blue shift in the absorption spectrum of ~8 nm.

**LA (97% all-*trans*, 3% 13-*cis*), DA (40% all-*trans*, 60% 13-*cis*), at pH 6.

##LA (79% all-*trans*, 21% 13-*cis*), DA (50% all-*trans*, 50% 13-*cis*), at pH 6.

§§LA (61% all-*trans*, 27% 13-*cis*, 9% 11-*cis*, 3% 9-*cis*), DA (84% all-*trans*, 16% 13-*cis*), at pH 6.

¶¶LA (73% all-*trans*, 27% 13-*cis*), DA (42% all-*trans*, 58% 13-*cis*), at pH 6.

‖‖LA (78% all-*trans*, 22% 13-*cis*), DA (78% all-*trans*, 22% 13-*cis*), at pH 6.

***LA (56% all-*trans*; 31% 13-*cis*; 4% 11-*cis*, 9% 9-*cis*), DA (63% all-*trans*; 33% 13-*cis*; 4% 9-*cis*) at pH 4.2. Isomeric composition has been shown to be pH-dependent (Turner et al., 1993).

###LA (47% all-*trans*; 34% 13-*cis*; 12% 11-*cis*, 7% 9-*cis*), DA (29% all-*trans*; 60% 13-*cis*; 8% 11-*cis*; 3% 9-*cis*) at pH 4.2.

§§§LA (61% all-*trans*, 29% 13-*cis*, 6% 11-*cis*, 4% 9-*cis*), DA (25% all-*trans*, 71% 13-*cis*, 3% 11-*cis* 1% 9-*cis*) at pH 4.2.

¶¶¶These mutants are reported to be either labile or conformationally invariant to light adaptation (Zhang et al., 1993).

procedures indicate that moving one of the distant non-hydrogen-bonded water molecules specified into hydrogen-bonding position with the imine proton lowers the energy of the total structure by 12–18 kcal mol^{-1}. Furthermore, the resultant binding site yields better agreement with spectroscopic experiment (error shifts from 0.426 to 0.389). In summary, then, our simulations provide strong evidence that water is directly hydrogen-bonded to the imine proton. We have no explanation for why a water molecule was not observed near the imine hydrogen in the study by Peyroula et al. (1997), when such a molecule was observed in the study by Luecke et al. (1998). Nor can we explain why the 1AP9 and 1BRX structures exhibit such significant differences in assignment of the Arg^{82} position. Further work will be required to clarify these interesting issues.

Conclusions of the model binding site studies

We conclude that a neutral protein binding site with Arg^{82} in an upward position represents the most realistic model for the light-adapted protein binding site. At ambient temperature, we view both U1 (or 1BRX) and U2 as realistic models, with a modest preference for U1 based on error (Table 2), energy (see above), and close agreement with the geometry observed in the diffraction studies by Luecke et al. (1998). Recent theoretical studies also support a model placing Arg^{82} "up" in light-adapted bacteriorhodopsin (Bashford and Gerwert, 1992; Edholm et al., 1995; Honig et al., 1995; Humphrey et al., 1994; Jahnig and Edholm, 1992; Nagel et al., 1997; Sampogna and Honig, 1994, 1996; Scharnagl and Fischer, 1994; Scharnagl et al., 1995; Schulten et al., 1995; Xu et al., 1996). However, none of these studies have examined the competition between a divalent metal and Arg^{82} for occupation of the chromophore-adjacent binding site, and these studies thus provide only conditional support for our conclusion. And it should be noted that the most recent ab initio study concludes that a divalent metal occupies the chromophore binding site (Pardo et al., 1998). Thus we seek additional insight by evaluating the

results of spectroscopic studies of proteins with modified Arg^{82} residues.

Spectroscopic properties of site-directed mutants involving Arg^{82}

In principle, site-directed mutagenesis (SDM) should provide an unequivocal answer to the question of whether Arg^{82} is interacting electrostatically with the chromophore. In practice, the numerous studies involving substitution of Arg^{82} in both the *Escherichia coli* and *H. salinarium* expression systems have yielded conflicting results. Some key spectroscopic studies involving Arg^{82} and other counterion mutants are presented in Table 3.

The difficulty in interpreting the SDM spectroscopic data is due to three complications. First, the ability to fully light-adapt the mutants is often compromised by the changes in the binding site, resulting in 9-*cis*, 11-*cis*, or 13-*cis* isomeric contamination (see footnotes to Table 3). The presence of these isomers often produces a blue-shifted absorption maximum. Second, the modification of a specific residue will often affect the positions and protonation states of other residues in a complex fashion. This observation is particularly relevant for a charged residue such as Arg^{82} and can produce long-range effects that are difficult to predict. Third, many of the studies were carried out using buffers and salts, which can donate charged counterions from the bath to mediate the removal of the charged Arg^{82} residue. It is known that both metal and organic cations can function to mediate the color of bacteriorhodopsin (e.g., Tan et al., 1996), and anions have been shown to bind and affect the spectroscopic characteristics of mutants involving the removal of negatively charged residues such as D85 and D212 (Marti et al., 1992).

Examination of the selected data presented in Table 3 demonstrates the problem of interpretation. First, we note that replacement of Arg^{82} with the hydrophilic residue Gln (R82Q) produces a red shift at pH 6 and a blue shift at pH 8. This pH dependence is due to titration of Asp^{85} (Subramaniam et al., 1990). At a nearly neutral pH of 7.3 in the dark-adapted *E. coli* expressed species, the effect is minimal (550–547 nm). One possibility is that at neutral pH the replacement of Arg^{82} produces a blue shift, the resulting protonation of Asp^{85} a red shift, and the small blue shift is a result of a near-cancellation of these two effects. In that regard, the blue form of the R82Q mutant (with protonated Asp^{85}) has properties quite similar to those of the R82Q/D85N mutant (Brown et al., 1993). Our analysis is complicated by the observation that the R82Q mutant behaves rather differently, depending upon the expression system. A similar problem attends analysis of the R82A ($Arg^{82} \rightarrow Ala^{82}$) data, where a strong pH effect is observed in the *H. salinarium*-expressed dark-adapted species.

It is interesting to note that R82Q/D212N (*E. coli*) and D212N (*H. salinarium*) yield an identical 8-nm red shift in the light-adapted species at pH 6–6.5. The R82Q/D212N mutant expressed in *H. salinarium* exhibits an even smaller red shift from the native protein in a wide pH range (3–10) (Brown et al., 1995b). In contrast, R82Q/D85N and D85N exhibit much larger red shifts of 18 nm and 48 nm, respectively, at pH 6.5–7.8 in the *H. salinarium*-expressed light-adapted species. The small red shift observed for D212N at neutral pH may be due to bound chloride (Marti et al., 1991, 1992), which is supported by the observation that at pH values higher than 7, D212N exhibits a 17-nm red shift relative to wild-type (Needleman et al., 1991). Although the above-noted complications invite caution, it seems clear that D85N generates a much larger red shift than D212N, and R82Q/D85N induces a larger red shift than R82Q/D212N. The following assumptions provide an attractive and internally consistent explanation:

1. Arg^{82} is in the "up" position and preferentially interacts with Asp^{212}.
2. Asp^{85} is the primary counterion interacting with the chromophore.
3. Neutral replacement of Asp^{212}, but not necessarily Asp^{85}, may cause Arg^{82} to move into a "down" position unless small anions are present.
4. If small anions (such as Cl^-) are available, removal of either Asp^{85} or Asp^{212} may cause these anions to enter the binding site at low pH, serving to neutralize the binding site and diminishing (or eliminating) the spectroscopic red shift.

Assumptions 1 and 2 explain why D85N produces a larger red shift (48 nm) than D212N (8–17 nm) and why R82Q/D85N produces a larger red shift (18 nm) than R82Q/D212N (0–8 nm). Assumption 1 explains why the red shifts of R82Q/D85N and D85N are different. The very large red shift observed for the D85N mutant may indicate that Arg^{82} stays up in the binding site, still interacting with Asp^{212}, to produce a positively charged binding site. However, the large red shift could also be accounted for by steric interactions or the inability of Asp^{212} to provide full electrostatic stabilization of the chromophore. Thus assumptions 3 and 4 equivocate regarding the motion of Arg^{82} upon Asp^{85} replacement (or protonation) and qualify the situation when anions are present. The above analysis suggests that U1 is the most realistic binding site for light-adapted bacteriorhodopsin. The U1 model is also calculated to have the lowest energy of the binding sites investigated here, with the exception of P1. Finally, we note that the U1 model is very similar to the model of Luecke et al. (1998), which yielded the best agreement with experiment of all of the diffraction-based models examined (Table 2).

Arg^{82} dynamics

The above analysis of Arg^{82} mutants suggests the possibility that Arg^{82} moves away from the binding site when Asp^{212} is protonated. This conformational reorganization would serve to maintain neutrality in the binding site. During the photocycle an event of greater electrostatic consequences occurs in which Asp^{85} becomes protonated and

Glu^{204} becomes deprotonated. Is it possible that this event could induce motion of Arg^{82}? We carried out MM2 calculations to investigate the dynamics of Arg^{82} in response to changes in the local electrostatic environment. It is known from experimental studies that the pK_a values of Asp^{85} and Glu^{204} are coupled so that at neutral pH one or the other residue, but never both, is protonated (Balashov et al., 1996; Brown et al., 1995a,b; Richter et al., 1996). Most of our calculations used the "Henderson coordinates" as a starting point, but we also carried out one set of calculations using the more recent model proposed by Luecke et al. (1998). In all cases, we monitored the motion of Arg^{82} as a function of the protonation states of Asp^{85} and Glu^{204}. All other regions of the protein were forced-neutral because of salt-bridge formation or adjustment of protonation state. The key results are shown in Fig. 9.

We conclude that protonation of Glu^{204} or coupling of Glu^{204} with a divalent metal cation will induce the motion of Arg^{82} up into the binding site, provided the extracellular surface has a net neutral or positive charge. In this regard, the simulations shown in Fig. 9 may represent the terminal kinetic sequence in the blue-to-purple transition studied by Fu et al. (1997). Thus, as a positively charged counterion neutralizes the extracellular surface through interaction, Arg^{82} shifts up to generate the electrostatic interactions that characterize the binding site of light-adapted bacteriorhodopsin.

Of equal interest is the motion of Arg^{82} during the latter stages of the photocycle. This issue has been studied in much less detail, and our investigation illustrates one significant difficulty. Our simulations indicate that if the protonation state of Asp^{85} and the chromophore are reversed (as in the M intermediate), the binding site remains neutral and Arg^{82} moves toward Asp^{212}, forming a stronger electrostatic coupling. In no simulations did Arg^{82} leave the binding site. However, if both the chromophore and Asp^{85} are protonated (as in the N intermediate), the dynamics of Arg^{82} are calculated to be hydration dependent. When 12 waters are equilibrated within the channel, protonation of Asp^{85} and the chromophore and deprotonation of Glu^{204} induced a shift of the Arg^{82} toward Asp^{212}, where it stayed for at least 600 ps at a temperature of 300 K. When the number of water molecules was reduced to five, however, the Arg^{82} residue eventually moved toward the extracellular surface to interact directly with Glu^{204} (Fig. 9 *e*). During this process, four specific regions of metastability were noted. We also carried out a calculation on 1BRX (Luecke et al., 1998), which has three waters explicitly positioned within this channel. The shift downward was completed in less than 100 ps, although we anticipate that more water molecules are actually present in this region, and hence our simulation will underestimate the translocation time. Our observation is consistent with a number of models of the photocycle involving motion of Arg^{82} toward the extracellular region during the latter stages of the photocycle (Balashov et al., 1993, 1995; Braiman et al., 1988; Rothschild, 1992; Scharnagl et al., 1995). We also carried out simulations using both the U1 and 1BRX models with the chromophore (13-*cis* unprotonated Schiff base) and $Asp^{85}H$ residues minimized to simulate the M intermediate. These studies were prompted by the observation of Dickopf and Heyn (1997) that Arg^{82} translocates down during the rise of the M intermediate. We observed no motion of the residue after 4-ns simulations for either model. Rather, we observed motion of Arg^{82} and Asp^{212} toward each other to form a stable salt bridge. Only after reprotonation of the chromophore (i.e., formation of the N intermediate) was a sufficient driving force present to induce downward motion of Arg^{82}. These simulations do not preclude the translocation of the Arg^{82} residue in the M intermediate, because the time scale of our simulations is too short. However, these results do suggest that if translocation of Arg^{82} during the formation of M is occurring, it is likely coupled to other (as yet undefined) processes.

COMMENTS AND CONCLUSIONS

We conclude that Arg^{82} is a primary counterion within the chromophore binding site and is interacting with either Asp^{85} and/or Asp^{212} in light-adapted bacteriorhodopsin. A water molecule is directly associated through hydrogen bonding with the imine proton on the chromophore, and this water molecule mediates the interaction of the negatively charged Asp^{85} and Asp^{212} residues with the protonated Schiff base chromophore. We conclude that the binding site of light-adapted bacteriorhodopsin is neutral and does not contain a divalent metal cation, as proposed previously. Our best fit is shown in Fig. 5 and is in good agreement with the binding site geometry predicted by Luecke et al. (1998).

The chromophore "$^1B_u{}^{*+}$" and "$^1A_g{}^{*-}$" states are extensively mixed in all of the binding site models studied, and yet these states exhibit significantly different configurational character. The lowest-lying "$^1B_u{}^{*+}$" state is dominated by single excitations (>76% for all models studied), whereas the second excited "$^1A_g{}^{*-}$" state is dominated by double excitations (>62% for all models studied, with extensive participation by spin-coupled triplet-triplet excitations). We can rule out the possibility of a negatively charged binding site, because such a site would produce a lowest-lying "$^1A_g{}^{*-}$" state, which is contrary to experimental observation (Birge and Zhang, 1990).

Molecular dynamics simulations indicate that when Glu^{204} is protonated, Arg^{82} will spontaneously translocate toward the chromophore binding site and directly stabilize Asp^{212} and, through a water molecule, Asp^{85}. Our simulations indicate that Arg^{82} will remain in the binding site through M, but not necessarily through N. Upon simultaneous protonation of both Asp^{85} and the chromophore, Arg^{82} will migrate down toward Glu^{204} at medium or lower levels of hydration. The process is relatively slow by molecular standards and requires over 250 ps ($T = 300$ K, five water molecules in the lower channel).

If Arg^{82} is the positively charged counterion mediating the chromophore binding site, what remains to be explained

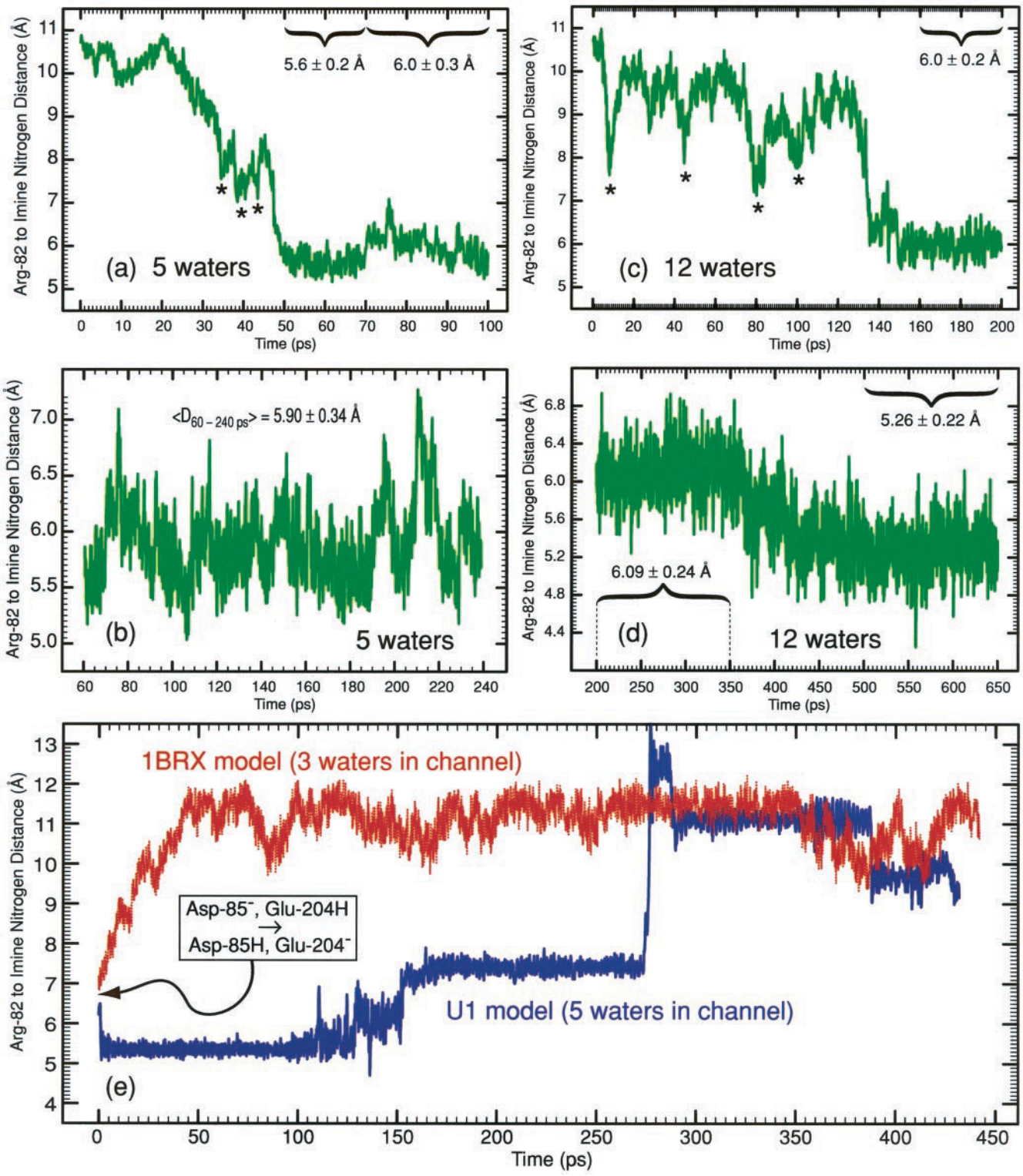

FIGURE 9 Molecular dynamics of Arg^{82} motion in response to changes in the protonation states of Asp^{85} and Glu^{204}. All simulations assumed a protonated chromophore. Simulations shown in green assumed Asp^{85-}:Asp^{212-}:$Glu^{204}H$ and the 2BRD coordinates (Grigorieff et al., 1996). The simulation shown in blue assumed the U1 structure (Fig. 5). The simulation shown in red assumed a starting geometry as proposed by Luecke et al. (1998). The vertical axis monitors the distance between the chromophore imine nitrogen atom and the closest nitrogen atom on the Arg^{82} side chain. In insets *a–d*, the specified number of water molecules was inserted inside the channel between Glu^{204} and Lys^{216}, the protein backbone was locked, and the structure was minimized. At time 0, the Glu^{204} residue was protonated, and the dynamics were followed by using an MM2 force field at a temperature of 300 K. The reverse situation was monitored in inset *e*, where the U1 structure (*dark blue*) or the Luecke et al. (1998) structure (*dark red*) served as the starting point, and at time 0 the protonation states of Asp^{85} and Glu^{204} were reversed, but the chromophore was kept protonated (as in the N intermediate). Dynamics with 12 waters (not shown) yielded no motion of Arg^{82} out of the binding site after 600 ps. The asterisks in insets *a* and *b* represent metastable states similar to U3. All simulations involving $Glu^{204}H$:Asp^{85-}:Asp^{212-} ended with U1- or U2-like geometries, with 300 K dynamics that included a nearly equal mixture of both.

is the origin of the microwave signal at ~9.7 GHz that accompanies formation of the M intermediate (Birge et al., 1996). This signal has been traced to a Ca(II) ion experiencing a change in environment characteristic of a decrease in binding constant. It is tempting to speculate that Glu^{204} is directly or indirectly involved in a Ca(II) binding site near the extracellular surface that is disturbed upon the protonation of this residue. We are testing this hypothesis both experimentally and theoretically.

The authors thank Richard Henderson and Janos Lanyi for providing us with the coordinates of bacteriorhodopsin resulting from their diffraction studies. We also thank Richard Needleman, Michael Ottolenghi, and Mudi Sheves for interesting and helpful discussions.

This work was supported in part by grants from the National Institutes of Health (GM-34548), the National Science Foundation (NSF) (CHE-96-0022N), and the W. M. Keck Foundation. CHM acknowledges a NSF postdoctoral fellowship in chemistry (CHE-95-04697).

REFERENCES

Alexiev, U., T. Marti, M. Heyn, H. Khorana, and P. Scherrer. 1994. Surface charge of bacteriorhodopsin detected with covalently bound pH indicators at selected extracellular and cytoplasmic sites. *Biochemistry.* 33:298–306.

Ames, J. B., S. R. Bolton, M. M. Netto, and R. A. Mathies. 1990. Ultraviolet resonance raman spectroscopy of bacteriorhodopsin: evidence against tyrosinate in the photocycle. *J. Am. Chem. Soc.* 112: 9007–9009.

Ames, J. B., M. Ros, J. Raap, J. Lugtenburg, and R. A. Mathies. 1992. Time-resolved ultraviolet resonance Raman studies of protein structure: applications to bacteriorhodopsin. *Biochemistry.* 31:5328–5334.

Ariki, M., D. Magde, and J. K. Lanyi. 1987. Metal ion binding sites of bacteriorhodopsin. *J. Biol. Chem.* 262:4947–4951.

Balashov, S., R. Govindjee, E. Imasheva, S. Misra, T. Ebrey, Y. Feng, R. Crouch, and D. Menick. 1995. The two pKa's of aspartate-85 and control of thermal isomerization and proton release in the arginine-82 to lysine mutant of bacteriorhodopsin. *Biochemistry.* 34:8820–8834.

Balashov, S., R. Govindjee, M. Kono, E. Imasheva, E. Lukashev, T. Ebrey, R. Crouch, D. Menick, and Y. Feng. 1993. Effect of the arginine-82 to alanine mutation in bacteriorhodopsin on dark adaptation, proton release, and the photochemical cycle. *Biochemistry.* 32:10331–10343.

Balashov, S. P., E. S. Imasheva, R. Govindjee, and T. G. Ebrey. 1996. Titration of aspartate-85 in bacteriorhodopsin: what it says about chromophore isomerization and proton release. *Biophys. J.* 70:473–481.

Bashford, D., and K. Gerwert. 1992. Electrostatic calculation of the pK_a values of ionizable groups in bacteriorhodopsin. *J. Mol. Biol.* 224: 473–486.

Birge, R. R. 1983. One-photon and two-photon excitation spectroscopy. *In* Ultrasensitive Laser Spectroscopy. Academic Press, New York. 109–174.

Birge, R. R. 1986. Two-photon spectroscopy of protein bound chromophores. *Acc. Chem. Res.* 19:138–146.

Birge, R. R., R. B. Barlow, Jr., and J. R. Tallent. 1992a. On the molecular origins of thermal noise in vertebrate and invertebrate photoreceptors. *In* Structures and Functions of Retinal Proteins. John Libbey Eurotext, Paris. 283–286.

Birge, R. R., J. A. Bennett, L. M. Hubbard, A. L. Fang, B. M. Pierce, D. S. Kliger, and G. E. Leroi. 1982. Two-photon spectroscopy of all-*trans* retinal. Nature of the low-lying states. *J. Am. Chem. Soc.* 104: 2519–2525.

Birge, R. R., D. S. K. Govender, K. C. Izgi, and E. H. L. Tan. 1996. Role of calcium in the proton pump of bacteriorhodopsin. Microwave evidence for a cation-gated mechanism. *J. Phys. Chem.* 100:9990–10004.

Birge, R. R., R. B. Gross, M. B. Masthay, J. A. Stuart, J. R. Tallent, and C. F. Zhang. 1992b. Nonlinear optical properties of bacteriorhodopsin and protein based two-photon three-dimensional memories. *Mol. Cryst. Liq. Cryst. Sci. Technol. Sec. B. Nonlinear Optics.* 3:133–147.

Birge, R. R., L. P. Murray, B. M. Pierce, H. Akita, V. Balogh-Nair, L. A. Findsen, and K. Nakanishi. 1985. Two-photon spectroscopy of locked-11-*cis* rhodopsin: evidence for a protonated Schiff base in a neutral protein binding site. *Proc. Natl. Acad. Sci. USA.* 82:4117–4121.

Birge, R. R., and B. M. Pierce. 1979. A theoretical analysis of the two-photon properties of linear polyenes and the visual chromophores. *J. Chem. Phys.* 70:165–178.

Birge, R. R., K. Schulten, and M. Karplus. 1975. Possible influences of a low-lying "covalent" excited state on the absorption spectrum and photoisomerization of 11-*cis* retinal. *Chem. Phys. Lett.* 31:451–454.

Birge, R. R., and C. F. Zhang. 1990. Two-photon spectroscopy of light adapted bacteriorhodopsin. *J. Chem. Phys.* 92:7178–7195.

Braiman, M., T. Mogi, T. Marti, L. Stern, H. Khorana, and K. Rothschild. 1988. Vibrational spectroscopy of bacteriorhodospin mutants: light-driven proton transport involves protonation changes of aspartic acid residues 85, 96 and 212. *Biochemistry.* 27:8516–8520.

Brown, L., L. Bonet, R. Needleman, and J. Lanyi. 1993. Estimated acid dissociation constants of the Schiff base, Asp^{85} and Arg^{82} during the bacteriorhodopsin photocycle. *Biophys. J.* 65:124–130.

Brown, L. S., J. Sasaki, H. Kandori, A. Maeda, R. Needleman, and J. K. Lanyi. 1995a. Glutamic acid 204 is the terminal proton release group at the extracellular surface of bacteriorhodopsin. *J. Biol. Chem.* 270: 27122–27126.

Brown, L. S., G. Varo, M. Hatanaka, J. Sasaki, H. Kandori, A. Maeda, N. Friedman, M. Sheves, R. Needleman, and J. K. Lanyi. 1995b. The complex extracellular domain regulates the deprotonation and reprotonation of the retinal Schiff base during the bacteriorhodopsin photocycle. *Biochemistry.* 34:12903–12911.

Buckert, U., and N. L. Allinger. 1982. Molecular Mechanics. American Chemical Society, Washington, DC.

Chronister, E. L., and M. M. El-Sayed. 1987. Time-resolved resonance Raman spectra of the photocycle intermediates of acid and deionized bacteriorhodopsin. *Photochem. Photobiol.* 45:507–513.

de Groot, H., S. Smith, J. Courtin, E. van den Berg, C. Winkel, J. Lugtenburg, R. Griffin, and J. Herzfeld. 1990. Solid-state ^{13}C and ^{15}N NMR study of the low pH forms of bacteriorhodopsin. *Biochemistry.* 29:6873–6883.

Dér, A., S. Száraz, R. Tóth-Boconádi, Z. Tokaji, L. Keszthelyi, and W. Stoeckenius. 1991. Alternative translocation of protons and halide ions by bacteriorhodopsin. *Proc. Natl. Acad. Sci. USA.* 88:4751–4755.

Dewar, M. J. S., and W. Thiel. 1977. Ground states of molecules. 38. The MNDO method. Approximations and parameters. *J. Am. Chem. Soc.* 99:4899–4917.

Dewar, M. J. S., E. G. Zoebisch, E. F. Healy, and J. J. P. Stewart. 1985. AM1: a new general purpose quantum mechanical molecular model. *J. Am. Chem. Soc.* 107:3902–3909.

Dick, B., and G. Hohlneicher. 1982. Importance of initial and final states as intermediate states in two-photon spectroscopy of polar molecules. *J. Chem. Phys.* 76:5755–5760.

Dickopf, S., and M. Heyn. 1997. Evidence for the first phase of the reprotonation switch of bacteriorhodopsin from time-resolved photovoltage and flash photolysis experiments on the photoreversal of the M-intermediate. *Biophys. J.* 73:3171–3181.

Dudek, M. J., and J. W. Ponder. 1995. Accurate modeling of the intramolecular electrostatic energy of proteins. *J. Comput. Chem.* 16:791–816.

Duñach, M., S. Berkowitz, T. Marti, Y.-W. He, S. Subramanian, H. G. Khorana, and K. J. Rothschild. 1990a. Ultraviolet-visible transient spectroscopy of bacteriorhdopsin mutants. Evidence for two forms of tyrosine-185 → phenylalanine. *J. Biol. Chem.* 265(28):16978–16984.

Duñach, M., T. Marti, H. Khorana, and K. Rothschild. 1990b. UV-visible spectroscopy of bacteriorhodopsin mutants: substitution of Arg^{82}, Asp^{85}, Tyr^{185}, and Asp^{212} results in abnormal light-dark adaptation. *Proc. Natl. Acad. Sci. USA.* 87:9873–9877.

Edholm, O., O. Berger, and F. Jahnig. 1995. Structure and fluctuations of bacteriorhodopsin in the purple membrane: a molecular dynamics study. *J. Mol. Biol.* 250:94–111.

El-Sayed, M. A., D. Yang, S.-K. Yoo, and N. Shang. 1995. The effect of different metal cation binding on the proton pumping in bacteriorhodopsin. *Isr. J. Chem.* 35:465–474.

Eyring, G., and R. Mathies. 1979. Resonance Raman studies of bathorhodopsin: evidence for a protonated Schiff base linkage. *Proc. Natl. Acad. Sci. USA.* 76:33–37.

Fischer, U. C., P. Towner, and D. Oesterheldt. 1981. Light induced isomerization, at acidic pH, initiates hydrolysis of bacteriorhodopsin to bacterio-opsin and 9-*cis*-retinal. *Photochem. Photobiol.* 33:529–537.

Fu, X., S. Bressler, M. Ottolenghi, T. Eliash, N. Friedman, and M. Sheves. 1997. Titration kinetics of Asp^{85} in bacteriorhodopsin: exclusion of the retinal pocket as the color-controlling cation binding site. *FEBS Lett.* 416:167–170.

Grigorieff, N., T. A. Ceska, K. H. Downing, J. M. Baldwin, and R. Henderson. 1996. Electron-crystallographic refinement of the structure of bacteriorhodopsin. *J. Mol. Biol.* 259:393–421.

Harada, I., T. Yamagishi, K. Uchida, and H. Takeuchi. 1990. Ultraviolet resonance Raman spectra of bacteriorhodopsin in the light-adapted and dark-adapted states. *J. Am. Chem. Soc.* 112:2443–2445.

Henderson, R., J. M. Baldwin, T. A. Ceska, F. Zemlin, E. Beckmann, and K. H. Downing. 1990a. Model for the structure of bacteriorhodopsin based on high-resolution electron cryo-microscopy. *J. Mol. Biol.* 213: 899–929.

Henderson, R., F. R. S. Schertler, and G. R. X. Schertler. 1990b. The structure of bacteriorhodopsin and its relevance to the visual opsins and other seven-helix G-protein coupled receptors. *Philos. Trans. R. Soc. Lond. B.* 326:379–389.

Herzfeld, J., S. K. Das Gupta, M. R. Farrar, G. S. Harbison, A. E. McDermott, S. L. Pelletier, D. P. Raleigh, S. O. Smith, C. Winkel, J. Lugtenburg, and R. G. Griffin. 1990. Solid-state ^{13}C NMR study of tyrosine protonation in dark-adapted bacteriorhodopsin. *Biochemistry.* 29:5567–5574.

Honig, B., M. Ottolenghi, and M. Sheves. 1995. Acid-base equilibria and the proton pump in bacteriorhodopsin. *Isr. J. Chem.* 35:429–446.

Humphrey, W., I. Logunov, K. Schulten, and M. Sheves. 1994. Molecular dynamics study of bacteriorhodopsin and artificial pigments. *Biochemistry.* 33:3668–3678.

Jahnig, F., and O. Edholm. 1992. Modeling of the structure of bacteriorhodopsin: a molecular dynamics study. *J. Mol. Biol.* 226: 837–850.

Jonas, R., and T. G. Ebrey. 1991. Binding of a single divalent cation directly correlates with the blue-to-purple transition in bacteriorhodopsin. *Proc. Natl. Acad. Sci. USA.* 88:149–153.

Kimura, Y., D. G. Vassylyev, A. Miyazawa, A. Kidera, M. Matsushima, K. Mitsuoka, K. Murata, T. Hirai, and Y. Fujiyoshi. 1997a. High resolution structure of bacteriorhodopsin determined by electron cyrstallography. *Photochem. Photobiol.* 66:764–767.

Kimura, Y., D. G. Vassylyev, A. Miyazawa, A. Kidera, M. Matsushima, K. Mitsuoka, K. Murata, T. Hirai, and Y. Fujiyoshi. 1997b. Surface of bacteriorhodopsin revealed by high-resolution electron crystallography. *Nature.* 389:206–211.

Koyama, Y., H. Nakasu, Y. Mukai, and F. Tokunaga. 1993. Isomerization of the retinylidene chromophore of bacteriorhodopsin in light adaptation: intrinsic isomerization of the chromophore and its control by the apo-protein. *Photochem. Photobiol.* 57:732–738.

Luecke, H., H. T. Richter, and J. K. Lanyi. 1998. Proton transfer pathways in bacteriorhodopsin at 2.3 Ångstrom resolution. *Science.* 280: 1934–1937.

Maeda, A., H. Kandori, Y. Yamazaki, S. Nishimura, M. Hatanaka, Y. Chon, J. Sasaki, R. Needleman, and J. Lanyi. 1997. Intramembrane signaling mediated by hydrogen bonding of water and carboxyl groups in bacteriorhodopsin and rhodopsin. *J. Biochem.* 121:399–406.

Maeda, A., I. Tatsuo, and T. Yoshizawa. 1981. Photoreaction of the acidified form of bacteriorhodopsin and its 9-*cis* derivative in purple membrane at low temperatures. *Photochem. Photobiol.* 33:559–565.

Marti, T., H. Otto, S. Rösselet, M. Heyn, and H. Khorana. 1992. Anion binding to the Schiff base of the bacteriorhodopsin mutants Asp^{85} to Asn/Asp^{212} to Asn and Arg^{82} to Gln/Asp^{85} to Asn/Asp^{212} to Asn. *J. Biol. Chem.* 267:16922–16927.

Marti, T., S. Rösselet, H. Otto, M. Heyn, and H. Khorana. 1991. The retinylidene Schiff base counterion in bacteriorhodopsin. *J. Biol. Chem.* 266:18674–18683.

Martin, C. H., and R. R. Birge. 1998. Reparameterizing MNDO for excited state calculations using ab initio effective Hamiltonian theory: application to the 2,4-pentadien-1-iminium cation. *J. Phys. Chem. A.* 102: 852–860.

Masuda, S., M. Nara, M. Tasumi, M. A. El-Sayed, and J. K. Lanyi. 1995. Fourier transform infrared spectroscopic studies of the effect of Ca^{2+} binding on the states of aspartic acid side chains in bacteriorhodopsin. *J. Phys. Chem.* 99:7776–7781.

McDermott, A. E., L. K. Thompson, C. Winkel, M. R. Farrar, S. Pelletier, J. Lugtenburg, J. Herzfeld, and R. G. Griffin. 1991. Mechanism of proton pumping in bacteriorhodopsin by solid-state NMR: the protonation state of tyrosine in the light-adapted and M states. *Biochemistry.* 30:8366–8371.

Metz, G., F. Siebert, and M. Engelhard. 1992. ASP_{85} is the only internal aspartic acid that gets protonated in the M intermediate and the purple-to-blue transition of bacteriorhodopsin: a solid-state ^{13}C CP-MAS NMR investigation. *FEBS Lett.* 303:237–241.

Misra, S., T. Ebrey, R. Crouch, and D. Menick. 1997. Charge movements in the 13-*cis* photocycles of the bacteriorhodopsin mutants R82K and R82Q. *Photochem. Photobiol.* 65:1039–1044.

Mortensen, O. S., and E. N. Svendsen. 1981. Initial and final molecular states as "virtual states" in two-photon processes. *J. Chem. Phys.* 74: 3185–3189.

Mowery, P. C., R. H. Lozier, Q. Chae, Y. W. Tseng, M. Taylor, and W. Stoeckenius. 1979. Effect of acid pH on the absorption spectra and photoreactions of bacteriorhodopsin. *Biochemistry.* 18:4100–4107.

Nagel, J., O. Edholm, O. Berger, and F. Jahnig. 1997. Investigation of the proton release channel of bacteriorhodopsin in different intermediates of the photocycle. A molecular dynamics study. *Biochemistry.* 36: 2875–2883.

Needleman, R., M. Chang, B. Ni, G. Váró, J. Fornés, S. White, and J. Lanyi. 1991. Properties of Asp^{212} to Asn bacteriorhodopsin suggest that Asp^{212} and Asp^{85} both participate in a counterion and proton acceptor complex near the Schiff base. *J. Biol. Chem.* 266:11478–11484.

Oesterhelt, D., and L. Schuhmann. 1974. Reconstitution of bacteriorhodopsin. *FEBS Lett.* 44:262–265.

Oesterhelt, D., and W. Stoeckenius. 1971. Rhodopsin-like protein from the purple membrane of *Halobacterium halobium*. *Nature New Biol.* 233: 149–152.

Oesterhelt, D., and W. Stoeckenius. 1974. Isolation of the cell membrane of *Halobacterium halobium* and its fractionation into red and purple membrane. *Methods Enzymol.* 31:667–678.

Ormos, P., K. Chu, and J. Mourant. 1992. Infrared study of the L, M and N intermediates of bacteriorhodopsin using the photoreaction of M. *Biochemistry.* 31:6933–6937.

Otto, H., T. Marti, M. Holz, T. Mogi, L. Stern, F. Engel, H. Khorana, and M. Heyn. 1990. Substitution of amino acids Asp^{85}, Asp^{212}, and Arg^{82} in bacteriorhodopsin affects the proton release phase of the pump and the pK of the Schiff base. *Proc. Natl. Acad. Sci. USA.* 87:1018–1022.

Pardo, L., F. Sepulcre, J. Cladera, M. Dunach, A. Labarta, J. Tejada, and E. Padros. 1998. Experimental and theoretical characterization of the high-affinity cation-binding site of the purple membrane. *Biophys. J.* 75:777–784.

Pebay-Peyroula, E., G. Rummel, J. P. Rosenbusch, and E. M. Landau. 1997. X-ray structure of bacteriorhodopsin at 2.5 Å from microcrystals grown in lipidic cubic phases. *Science.* 277:1676–1681.

Renthal, R., Y. Chung, R. Escamilla, L. Brown, and J. Lanyi. 1997. Guanidinium restores the chromophore but not rapid proton release in bacteriorhodopsin mutant R82Q. *Biophys. J.* 73:2711–2717.

Richter, H. T., L. S. Brown, R. Needleman, and J. K. Lanyi. 1996. A linkage of the pKa's of Asp^{85} and Glu^{204} forms part of the reprotonation switch of bacteriorhodopsin. *Biochemistry.* 35:4054–4062.

Roepe, P. D., P. L. Ahl, J. Herzfeld, J. Lugtenburg, and K. J. Rothschild. 1988. Tyrosine protonation changes in bacteriorhodopsin. A Fourier transform infrared study of br_{548} and its primary photoproduct. *J. Biol. Chem.* 263:5110–5117.

Rothschild, K. 1992. FTIR difference spectroscopy of bacteriorhodopsin: toward a molecular model. *J. Bioenerg. Biomembr.* 24:147–167.

Rothschild, K. J., M. S. Braiman, Y.-W. He, T. Marti, and H. G. Khorana. 1990. Vibrational spectroscopy of bacteriorhodopsin mutants. Evidence for the interaction of aspartic acid 212 with tyrosine 185 and possible role in the proton pump mechanism. *J. Biol. Chem.* 265(28): 16985–16991.

Sakmar, T. P., R. R. Franke, and H. G. Khorana. 1989. Glutamic acid 113 serves as the retinylidene Schiff base counterion in bovine rhodopsin. *Proc. Natl. Acad. Sci. USA.* 86:8309–8313.

Sampogna, R., and B. Honig. 1996. Electrostatic coupling between retinal isomerization and the ionization state of Glu^{204}: a general mechanism for proton release in bacteriorhodopsin. *Biophys. J.* 71:1165–1171.

Sampogna, R. V., and B. Honig. 1994. Environmental effects on the protonation states of active site residues in bacteriorhodopsin. *Biophys. J.* 66:1341–1352.

Scharnagl, C., and S. F. Fischer. 1994. Proton release pathway in bacteriorhodopsin: molecular dynamics and electrostatic calculations. *Int. J. Quantum Chem. Biol. Symp.* 21:33–56.

Scharnagl, C., J. Hettenkofer, and S. Fischer. 1995. Electrostatic and conformational effects on the proton translocation steps in bacteriorhodopsin: analysis of multiple M structures. *J. Phys. Chem.* 99:7787–7800.

Schulten, K., W. Humphrey, I. Logunov, M. Sheves, and D. Xu. 1995. Molecular dynamics studies of bacteriorhodopsin's photocycle. *Isr. J. Chem.* 35:447–464.

Schulten, K., J. Ohmine, and M. Karplus. 1976. Correlation effects in the spectra of polyenes. *J. Chem. Phys.* 64:4422–4437.

Stern, L., and H. Khorana. 1989. Structure-function studies on bacteriorhodopsin. X. Individual substitutions of arginine residues by glutamine affect chromophore formation, photocycle and proton translocation. *J. Biol. Chem.* 264:14202–14208.

Stewart, J. J. P. 1989. Optimization of parameters for semiempirical methods. *J. Comput. Chem.* 10:221–245.

Stoeckenius, W., and R. Bogomolni. 1982. Bacteriorhodopsin and related pigments of Halobacteria. *Annu. Rev. Biochem.* 52:587–616.

Stuart, J. A., B. W. Vought, C. F. Zhang, and R. R. Birge. 1995. The active site of bacteriorhodopsin. Two-photon spectroscopic evidence for a positively charged chromophore binding site mediated by calcium. *Biospectroscopy.* 1:9–28.

Subramaniam, S., T. Marti, and H. Khorana. 1990. Protonation state of Asp (Glu) 85 regulates the purple-to-blue transition in bacteriorhodopsin mutants Arg 82 to Ala and Asp 85 to Glu: the blue form is inactive in proton translocation. *Proc. Natl. Acad. Sci. USA.* 87:1013–1017.

Sweetman, L. L., and M. A. El-Sayed. 1991. The binding site of strongly bound Eu^{3+} in Eu^{3+}-regenerated bacteriorhodopsin. *FEBS Lett.* 282: 436–440.

Tallent, J. R., J. R. Birge, C. F. Zhang, E. Wenderholm, and R. R. Birge. 1992a. Conformational energetics and excited state level ordering in 11-*cis* retinal. *Photochem. Photobiol.* 56:935–952.

Tallent, J. R., E. Q. Hyde, L. A. Findsen, G. C. Fox, and R. R. Birge. 1992b. Molecular dynamics of the primary photochemical event in rhodopsin. *J. Am. Chem. Soc.* 114:1581–1592.

Tallent, J. R., J. A. Stuart, Q. W. Song, E. J. Schmidt, C. H. Martin, and R. R. Birge. 1998. Photochromism in dried polymer films incorporating the deionized blue membrane form of bacteriorhodopsin. *Biophys. J.* 75:1619–1634.

Tan, E. H. L., D. S. K. Govender, and R. R. Birge. 1996. Large organic cations can replace Mg^{2+} and Ca^{2+} ions in bacteriorhodopsin and maintain proton pumping ability. *J. Am. Chem. Soc.* 118:2752–2753.

Thiel, W. 1988. Semiempirical methods: current status and perspectives. *Tetrahedron.* 44:7393–7408.

Turner, G., L. Miercke, T. Thorgeirsson, D. Kliger, M. Betlach, and R. Stroud. 1993. Bacteriorhodopsin D85N: three spectroscopic species in equilibrium. *Biochemistry.* 32:1332–1337.

Xu, D., C. Martin, and K. Schulten. 1996. Molecular dynamics study of early picosecond events in the bacteriorhodopsin photocycle: dielectric response, vibrational cooling and the J, K intermediates. *Biophys. J.* 70:453–460.

Yamazaki, M., J. Goodisman, and R. R. Birge. 1998. Quadratic electrooptic effects in bacteriorhodopsin. Measurement of $\gamma(-\omega; 0, 0, \omega)$ in dried gelatin thin films. *J. Chem. Phys.* 108:5876–5887.

Zerner, M. C. 1990. Semiempirical molecular orbital methods. *In* Reviews in Computational Chemistry. VCH Publishers, New York. 313–365.

Zhang, N. Y., and M. A. El-Sayed. 1993. The C-terminus and the Ca^{2+} low-affinity binding sites in bacteriorhodopsin. *Biochemistry.* 32: 14173–14175.

Zhang, Y. N., M. A. El-Sayed, M. L. Bonet, J. K. Lanyi, M. Chang, B. Ni, and R. Needleman. 1993. Effects of genetic replacements of charged and H-bonding residues in the retinal pocket on Ca^{2+} binding to deionized bacteriorhodopsin. *Proc. Natl. Acad. Sci. USA.* 90:1445–1449.

Zhang, Y. N., L. L. Sweetman, E. S. Awad, and M. A. El-Sayed. 1992. Nature of the individual Ca^{2+} binding sites in Ca^{2+}-regenerated bacteriorhodopsin. *Biophys. J.* 61:1201–1206.

Zhukovsky, E. A., and D. D. Oprian. 1989. Effect of carboxylic acid side chains on the absorption maximum of visual pigments. *Science.* 246: 928–931.